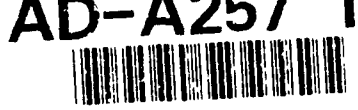

(2)

NAVAL POSTGRADUATE SCHOOL
Monterey, California

THESIS

MATHEMATICAL MODEL AND COMPUTER ALGORITHM
FOR TRACKING COASTAL STORM CELLS FOR
SHORT TERM TACTICAL FORECASTS

by

Carl A. Carpenter

September, 1992

Thesis Advisors: Carlyle H. Wash
Micheal J. Pastore

Approved for public release; distribution is unlimited.

UNCLASSIFIED
SECURITY CLASSIFICATION OF THIS PAGE

REPORT DOCUMENTATION PAGE

Form Approved
OMB No. 0704-0188

1a. REPORT SECURITY CLASSIFICATION UNCLASSIFIED	1b. RESTRICTIVE MARKINGS
2a. SECURITY CLASSIFICATION AUTHORITY	3 DISTRIBUTION / AVAILABILITY OF REPORT Approved for public release; distribution unlimited
2b. DECLASSIFICATION / DOWNGRADING SCHEDULE	
4 PERFORMING ORGANIZATION REPORT NUMBER(S)	5 MONITORING ORGANIZATION REPORT NUMBER(S)
6a. NAME OF PERFORMING ORGANIZATION Naval Postgraduate School 6b. OFFICE SYMBOL (If applicable) 3A	7a. NAME OF MONITORING ORGANIZATION Naval Postgraduate School
6c. ADDRESS (City, State, and ZIP Code) Monterey, CA 93943-5000	7b. ADDRESS (City, State, and ZIP Code) Monterey, CA 93943-5000
8a. NAME OF FUNDING / SPONSORING ORGANIZATION 8b. OFFICE SYMBOL (If applicable)	9 PROCUREMENT INSTRUMENT IDENTIFICATION NUMBER
8c. ADDRESS (City, State, and ZIP Code)	10 SOURCE OF FUNDING NUMBERS PROGRAM ELEMENT NO / PROJECT NO / TASK NO / WORK UNIT ACCESSION NO

11 TITLE (Include Security Classification)
MATHEMATICAL MODEL AND COMPUTER ALGORITHM FOR TRACKING COASTAL STORM CELLS FOR SHORT TERM TACTICAL FORECASTS

12. PERSONAL AUTHOR(S)
CARPENTER, Carl A.

13a TYPE OF REPORT	13b TIME COVERED	14 DATE OF REPORT (Year, Month, Day)	15 PAGE COUNT
Master's Thesis	FROM _____ TO _____	September 1992	109

16 SUPPLEMENTARY NOTATION The views expressed in this thesis are those of the author and do not reflect the official policy or position of the Department of Defense or the U.S. Government.

17 COSATI CODES			18 SUBJECT TERMS (Continue on reverse if necessary and identify by block number)
FIELD	GROUP	SUB-GROUP	Rain Cell Tracking; Kalman Filter

19 ABSTRACT (Continue on reverse if necessary and identify by block number) An algorithm has been developed for real-time forecasting of precipitation storm cell movement over water. The key to the algorithm is the Kalman filter tracking model which is continually updating the mean value and error covariance matrix of a cell's centroid position from past measurements. The algorithm was developed and applied to precipitation cells to evaluate the advantages of utilizing an optimal recursive processing program to assist in making short term tactical forecasts. This tracking algorithm was designed for use in a stand alone desktop computer. All of the real-time tracking data was detected by a land-based radar system. The thesis results suggest that for short term forecasting the Kalman filter can produce some improvements over other tracking models, but further refinement in identifying the storm cell center and mathematically identifying the area of extent of each individual cell is needed. Other possible improvements to the tracking algorithm might include a methodology to identify what meteorological parameters need to be included in the motion model. Incorporating those parameters into the Kalman error

20 DISTRIBUTION / AVAILABILITY OF ABSTRACT ☒ UNCLASSIFIED/UNLIMITED ☐ SAME AS RPT ☐ DTIC USERS	21- ABSTRACT SECURITY CLASSIFICATION UNCLASSIFIED
22a NAME OF RESPONSIBLE INDIVIDUAL WASH, Carlyle H.	22b TELEPHONE (Include Area Code) 408-646-2295 / 22c OFFICE SYMBOL MR/Wx

DD Form 1473, JUN 86 *Previous editions are obsolete*
S/N 0102-LF-014-6603

SECURITY CLASSIFICATION OF THIS PAGE
UNCLASSIFED

matrices will produce substantial improvements to the present storm cell tracking programs. An examination of the Kalman tracker predictions and the storm cell's radar position reveal a mean prediction centroid error for 30 minute predictions of approximately 5.81 km with a standard deviation of 3.64 km.

Approved for public release; distribution is unlimited.

Mathematical Model and Computer Algorithm
for Tracking Coastal Storm Cells for
Short Term Tactical Forecasts

by

Carl A. Carpenter
Lieutenant Commander, United States Navy
B.S , Oregon State University, 1980

Submitted in partial fulfillment
of the requirements for the degree of

MASTER OF SCIENCE IN APPLIED SCIENCE

from the

NAVAL POSTGRADUATE SCHOOL
September 1992

Author: 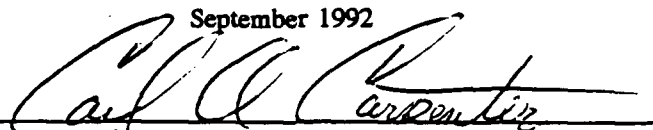
Carl A. Carpenter

Approved by: 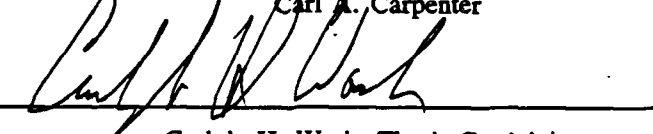
Carlyle H. Wash, Thesis Co-Advisor

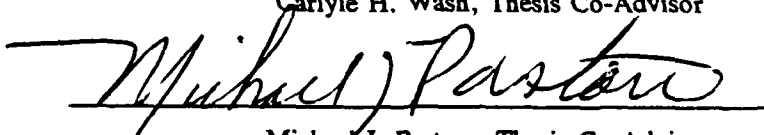
Micheal J. Pastore, Thesis Co-Advisor


William J. Walsh, Second Reader

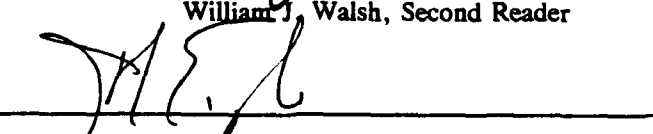
James N. Eagle, Chairman Antisubmarine Warfare Academic Group

ABSTRACT

An algorithm has been developed for near real-time forecasting of precipitation storm cell movement over water. The key to the algorithm is the Kalman filter tracking model which is continually updating the mean value and error covariance matrix of a cell's centroid position from past measurements. The algorithm was developed and applied to precipitation cells to evaluate the advantages of utilizing an optimal recursive processing program to assist in making short term tactical forecasts. This tracking algorithm was designed for use in a stand alone desktop computer. All of the real-time tracking data was detected by a land-based radar system. The thesis results suggest that for short term forecasting the Kalman filter can produce some improvements over other tracking models, but further refinement in identifying the storm cell center and mathematically identifying the area of extent of each individual cell is needed. Other possible improvements to the tracking algorithm might include a methodology to identify what meteorological parameters need to be included in the motion model. Incorporating those parameters into the Kalman error matrices will produce substantial improvements to the present storm cell tracking programs. An examination of the Kalman tracker predictions and the storm cell's radar position reveal a mean prediction centroid error for 30 minute predictions of approximately 5.81 km with a standard deviation of 3.64 km.

THESIS DISCLAIMER

The reader is cautioned that computer programs developed in this research may not have been exercised for all cases of interest. While every effort has been made, within the time available, to ensure that the programs are free of computational and logic errors, they cannot be considered validated. Any application of these programs without additional verification is at the risk of the user.

TABLE OF CONTENTS

LIST OF TABLES

LIST OF FIGURES

ACKNOWLEDGEMENT

I wish to express my sincerest thanks to Mike Pastore of the Naval Research Laboratory for providing encouraging guidance, patience, and his ability to always track me down. His reassurance that there was light at the end of the tunnel made what has been the most stressful part of my studies a positive experience.

A special appreciation goes to Professor Chuck Wash for his most valuable insight into the meteorological aspect of this thesis.

Valuable technical guidance was provided by Dr. Andreas Goroch of the Naval Research Laboratory. His willingness to give up the use of his computers and even his office is deeply appreciated. Thanks, Andy.

Finally, thanks to Maria, Rachel and Anthony for understanding why dad couldn't be at all the school activities and sports games. Now we can go home.

I. INTRODUCTION

A. PROBLEM STATEMENT

Precipitation storm clouds are routinely tracked by radar in an attempt to predict their course and speed and project their probable track over land and water. This is a standard shipboard tactical procedure This thesis develops a mathematical model and computer program for predicting precipitation movement over water of in situ storm cells for short term tactical forecasts (nowcasts) on the order of 30 minutes to two hours.

B. BACKGROUND

There is a need within the navy, and particularly the surface warfare community, for the ability to predict precipitation movement accurately for short range coastal tactical forecasts. Several critical shipboard evolutions are hampered by foul weather. The knowledge of impending precipitation storms can drive the time schedule of many precision navigation evolutions such as entering and leaving a port. The chances of a mishap, during those navigation events, are greatly increased when a ship's Captain is denied valuable navigation inputs (visual, audible, and in some cases even radar). The wind associated with intense storm cells is

another consideration, especially when negotiating narrow restricted channels with heavy two way shipping traffic.

Ship, aircraft, and personnel safety are other areas where precipitation tracking would be useful. Precipitation storms can hamper the launching and recovering of aircraft on board air capable vessels. The knowledge of a storm's estimated track can assist a Captain in determining the best flight schedule and/or ship location to prevent the hazardous foul weather air operations. Likewise, small boat operations for torpedo recovery during ASW exercises is another area of safety where precipitation nowcasts would be useful.

Anti-submarine (ASW) operations also are affected by adverse weather conditions. Precipitation storms may change the reverberation conditions used when calculating the search capability of an active sonar system and thus cause those calculations to be inaccurate. The combination of increased wave action and rainfall will hamper a ships' visual detection capability. The impact of the precipitation droplets on the ocean surface will increase the oceans' ambient noise and may be a source of reverberation which complicates the surface reflected sound propagation paths of the sonar equation.

Presently only a limited precipitation prediction capability is available to the Battle Group commander, via his assigned meteorological personnel detachment. The present precipitation tracking capability allows the Battle Group commander to predict the results of his units performances in

a multitude of missions. However, for the single small combatant this prediction capability is currently reduced to a one or two paragraph of weather predictions (in message format only) for the general area the ship is operating.

In 1990, a program was started to evaluate the effectiveness of providing real-time environmental support to the small combatant ships by the Oceanographer of the Navy, OP-096 [REF. 1]. This was the Integrated Oceanographic Tactical Aid (IOTA) program, which demonstrated environmental support onboard the USS MILLER (FF-1091). Since the operators of such a system are normally assigned shipboard personnel, they can not expected to be meteorological experts. The system must allow the users to modify the input and output results of the environmental sensors to make them tactically useful to the small combatant. The IOTA test program found many of the proposed meteorological products useful. The use of real-time radar rain display from shore radars had such great potential to Naval combatants that a demonstration weather Doppler radar system was installed on USS MILLER. [Ref. 2]. One of the problems identified from the doppler radar was the inability to estimate storm cell course/speed and size.

C. OBJECTIVES

The major thrust of this thesis deals with the problem of predicting the track and location of precipitation cells. It

analyzes whether a Kalman filter algorithm can use information data obtained from a weather radar to predict the tracks and probability area of storm cells. This thesis used storm data received from the National Weather service S-band radar sites in the RADAC network (system details in Appendix A). It is not the purpose of this thesis to address the multitude of problems inherent with the procurement of hardware needed to give naval vessels the independent ability to detect the storm cells (an inexpensive weather radar system was installed on USS MILLER in 1990/1991).

- Gather actual time series radar precipitation data and meteorological data.
- Identify an algorithm to transfer real-time precipitation storm cell data from the measuring system to an analysis computer.
- Develop a simple mathematical algorithm to describe the location and motion of storm cell for short term forecasting purposes.
- Evaluate the potential for computer graphics algorithms to represent the precipitation storm cell as a mathematical model for evaluation against actual data.
- Develop a simple precipitation storm cell tracking algorithm using the mathematical model developed above.

II. PRECIPITATION STORM CELL DETECTION AND TRACKING

A. RADAR PRECIPITATION STORM DETECTION

It has been known for many years that a radar's performance is considerably affected by weather (especially rainfall). The emitted radar energy interacts with the storm cells, and particularly rain storm cells. Some of the energy is scattered in many different directions and some of the energy is absorbed by the rain droplets [Ref. 3]. This depends on of the radar's wavelength and the droplet size distribution. As a result some radars have been developed with modes that enhance their ability to detect precipitation. The shorter the wavelength, the better the radar system is at detecting storm structures, particularly precipitation storm cells.

1. Resolution of radar beams

The air surveillance radar is designed for a wide area search with a high probability of detection of aircraft at all altitudes. Therefore, the older air surveillance radar used a high power, low frequency, wide beam transmitter to cover the largest area with each search beam. This wide beam transmission makes it difficult to determine bearing resolution between two radar contacts. The lack of precise bearing accuracy makes the older air surveillance radars poor

weather detection radars. The newer air surveillance radars, like SPY-1 type radar, show a great potential but would require some signal processing modifications.

A weather radar uses a higher frequency and as narrow a beam as practical in order to concentrate the signal energy and provide better resolution. Accurate bearing and range measurements of precipitation cells is essential to any tracking algorithm for forecasting the storm's track.

The air surveillance radar is designed for a wide area search utilizing high power, low frequency, wide beam transmission, is only slightly affected by the raindrops in the precipitation systems. Therefore, detection of storm structures by these high power, low frequency radars is very difficult and even if a detection were made the information about the rain would be limited. Radars with wavelengths of 20 cm and shorter were found to be reflected by raindrops, light rain, and even drizzle. The shorter the wavelength, the stronger the effect precipitation had on the radar signal, and thus the shorter the range of detection. This characteristic of short wavelength radars make them of primary interest to meteorological forecasters for their weather tracking needs.

2. Attenuation of weather radar beams

Selection of a weather tracking radar solely on the basis of its ability to detect the smallest precipitation clouds has drawbacks. The exact amount of attenuation depends

on the radar's wavelength, the size of the precipitation particles, and the intensity of the rainstorm. The shorter wavelength radars suffer much greater attenuation that the longer wavelengths. Attenuation increases as the fourth power of the radar wavelength [Ref. 3]. Effect of precipitation attenuation of a 10 cm or longer radar wave is considered negligible [Ref. 4]. A 3 to 5 cm wavelength radars would very precisely identify the edge of a precipitation storm nearest the radar, but because of attenuation the radar would be unable to determine the location of the farthest edge of the storm. Therefore, the size of the precipitation storm would not be available to the user. A compromise between the shorter wavelength (3 - 5 cm) radars and the longer wavelength (23 - 76 cm) radars has made the 10 cm radars the most commonly used radar for weather tracking.

B. PRECIPITATION STORM TRACKING RESEARCH

Crane discusses the radar storm cell detection and tracking algorithm that are currently being used in modern weather radar technology today [Ref. 5]. One of the first applications of a tracking algorithm to forecast storm cell tracks was reported by Hilst and Russo in 1960. During the following years several other tracking algorithms were developed and tested. These early attempts calculated a single direction and velocity for the entire data field [Ref. 6]. These algorithms worked well where the storm cells were

neither growing nor dissipating and the winds did not vary greatly with height. A problem arose when there are large deviation in cell velocity for the entire field. This problem would result in less accurate, more erratic, track calculations for the field center of mass [Ref. 5]. This effort will apply the Kalman filter to improve the accuracy of cell forecasting.

III. STORM CELL LOCATION AND TRACKING TIME SERIES

A. GENERAL PROCEDURES

1. Obtaining the storm cell data for the tracking algorithm

Real-time radar data from coastal land-based radar sites was used as input to the Kalman filter tracking algorithm developed for this thesis. The radar images were obtained from three east coast radar sites (Atlantic City NJ, Cape Hatteras NC, and Charleston SC, see Table I) and the radar data was transmitted to the Naval Postgraduate School via commercial phone modem. Only rain cell data over water was studied.

Each sequence of radar images collected by the RADAC Model 1000 system was digitally saved and displayed on a color monitor. The RADAC system is capable of storing a maximum of 15 unique radar images. This capability allows a user to retrieve a sequence of radar images for a period ranging from 45 minutes to six hours and 45 minutes. The number of radar images collected for a single storm cell was never controlled by the storage capacity of the RADAC system, but by rather the time period during which a user would obtain dedicated access to the Kavouras network by phone modem. The maximum access

time allowed to collect the data sets used for this thesis was approximately two hours.

After the data series were retrieved, each stored image was converted to a hard-copy output because of limited available technical equipment. These analog images of the storm cells were converted to binary digital data files using a Hewlett Packard Scanjet Plus. This procedure is not as good as getting raw digital images, but it is an early test of the concept. The desired procedure is for navy ships to obtain their own real-time radar images for use with future storm tracking algorithms on a shipboard stand alone computers.

Table I LATITUDE AND LONGITUDE LOCATION OF THE WEATHER RADAR SITES.

Radar Site Location	Latitude	Longitude
Atlantic City, NJ	39.45°N	074.56°W
Cape Hatteras, NC	35.26°N	075.55°W
Charleston, SC	32.9°N	080.03°W

2. Obtaining other supporting meteorological data

This thesis uses meteorological data received from the Navy Oceanographic Data Distribution System (NODDS) to support the results of the tracking algorithm. NODDS provides the

capability to define an area of interest and display many different types of conventional data for that area. NODDS can display up to three different meteorological products on a single screen display [Ref. 7]. To help support the results of the tracking algorithm, the synoptic reports, surface pressure, surface wind, 850MB wind, 700MB wind, and 500MB wind products were obtained from the NODDS.

B. STORM CELL TRACK AND OBSERVED METEOROLOGICAL DATA

Fifteen days of storm data were gathered over the period of 08 August to 04 October 1991. From these 15 days, six days of individual storm cells were identified as candidates for tracking evaluation. Appendix B contain the collection of the initial storm picture received via phone modem from the Kavouras radar network.

IV. THE ANALYSIS ALGORITHM

A. THE STORM CELL MODELING AND TRACKING TECHNIQUE

The main purpose of this thesis is to explore the prediction skill of a Kalman filter tracking algorithm applied to the movement and area of extent of precipitation storm cells over water.

1. Mathematical modeling of the storm cells

To enhance and define the precipitation storm cell area in each digital data file (radar picture), this thesis uses the *Image-Pro Plus (ver 1.01)* image processing software [Ref. 8].

The software filters each image using a choice of filters. A three-pass morphological filter was found to be the most effective in removing small scale variabilities in the storm cell images. The filtering removes the high spatial frequency information for a particular storm cell presenting a solid return on the radar image for later cluster analysis [Ref. 8].

One of the initial problems of the storm cell modeling technique is determining how to define the shape of the storm cell. Several tactical display systems currently being used in the navy (JOTS, STICCS, and FFISTS) use elliptical shape to represent the degree of uncertainty of a contact's position.

This thesis uses *Image-Pro Plus* to approximate an elliptical shape for each predominant storm cell. *Image-Pro Plus* calculates and displays the ellipse that best represent each major "filtered" storm cell image [Ref. 8]. The result is definition of the ellipse centroid position and major/minor axis. An example of the elliptical approximation by *Image-Pro Plus* is shown in Figure 1.

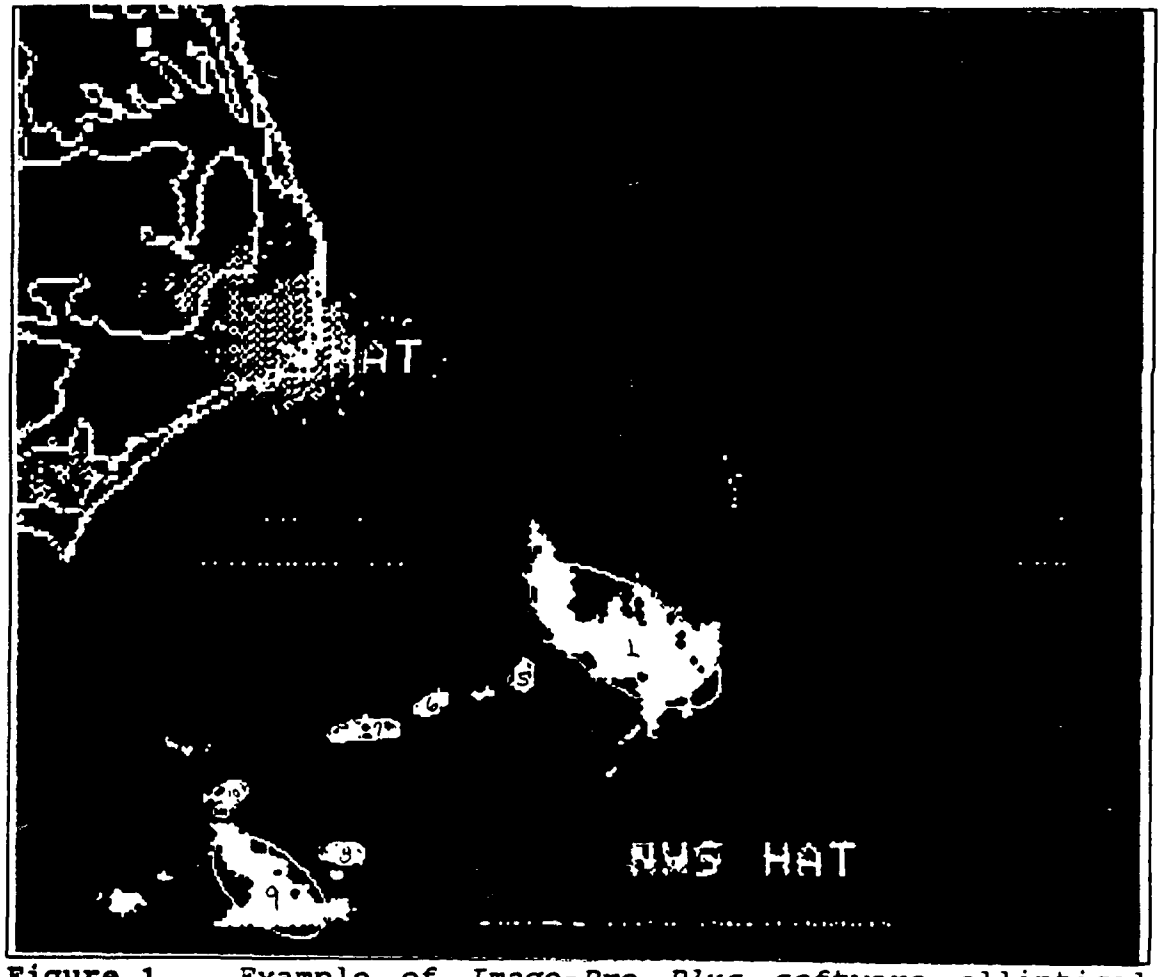

Figure 1. Example of *Image-Pro Plus* software elliptical approximation

2. Position, movement, growth and decay of the precipitation storm cell

Once the storm cell shapes have been defined this input data is used in the tracking algorithm to they are used to forecast the track of each major storm cell ellipse and to predict the future size of the storm cell. This is accomplished by providing the Kalman filter tracking algorithm with pertinent tracking data for each major storm ellipse from each set of radar pictures. For each ellipse *Image-Pro Plus* prepares a variety of statistics and stores the results in a data file. The most important calculations include the non-dimensional location of the centroid, non-dimensional length of the major and minor axes, and the angular orientation of the major axis of each ellipse. The location of the centroid of each ellipse is considered to be the center position of the storm cell (this was a critical assumption which resulted in significant difficulties because of the cell dynamics). This thesis uses a Kalman filter algorithm that uses the present centroid location of the storm cell and a statistical algorithm to forecast the dimension of the major and minor axis, and orientation of the ellipse representing the storm.

Each statistic in the storm data set will have some variance associated with its state vector. These variances are used by the statistical algorithm to find the uncertainty in each calculation of the storm cell size. Each successive area of uncertainty will result in expansion or contraction of

the next approximation of the storm cells' position and shape. This growth or decay of the shape of the storm cell could possible affect the model's predicted location area.

B. THE KALMAN FILTER TECHNIQUE

1. General theory

The Kalman filter is a dynamic transformation which combines some prior knowledge about an object's dynamic and random motion characteristics, the error covariance, and the measurement data for an object forecast the contact's position some time in the future (Figure 8).

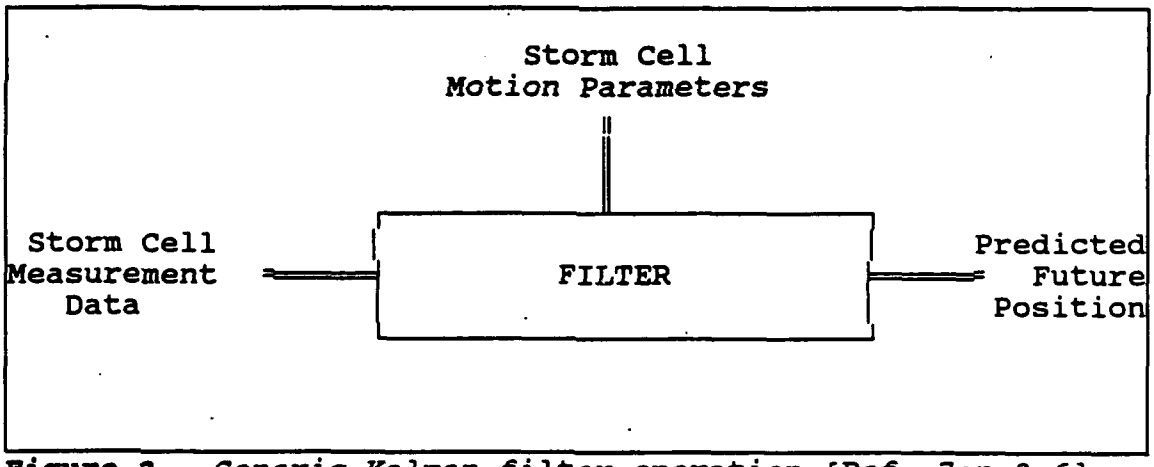

Figure 2. Generic Kalman filter operation [Ref. 7:p.3-6]

For the Kalman filter to successfully track a moving contact, the motion used to predict a contact's future position must contain both a dynamic part and a random part. The dynamic portion of the storm cell's motion model

incorporates the deterministic numerical process of solving the linear differential equation [Ref. 7]. The random portion of the storm cell's motion model must be considered if the filter is to attempt to predict the random maneuvers of a sometimes erratically moving storm cell.

The general Kalman filter algorithm is separated into two basic steps [Ref. 9:p. 1]:

- The movement step
- The measurement step

The movement step shows how the state of the system changes between measurements. The movement step is based upon the system model. It incorporates the way the system actually changes between measurements, along with a random noise which exists in real data.

The measurement step produces a new state vector estimate. The variables in the state vector estimate include the storm cell's location (latitude and longitude) and velocity in the north-south and east-west directions.

2. System model

A state vector matrix (X_k) contains values that uniquely describe each specific storm cell at a given time, k. The matrix contains values for the centroid location storm

cell and the storm cell's velocity in two dimensions. The state matrix is shown below in its mathematical form

$$\mathbf{X}_k = \begin{bmatrix} x \\ y \\ U_x \\ U_y \end{bmatrix} \quad . \tag{4.1}$$

The Kalman filter process uses the current state vector and a random variable to predict the updated state vector matrix ($\mathbf{X}_{k+1}$) using

$$\mathbf{X}_{k+1} = \phi\mathbf{X}_k + W \quad , \tag{4.2}$$

where:

$\mathbf{X}_k$ ⇒ The present state vector, $\mathbf{X}_k \sim N(\mu,\sigma) \sim R^n$

$\mathbf{X}_{k+1}$ ⇒ The updated state vector, $\mathbf{X}_k \sim N(\mu',\sigma') \sim R^n$

ϕ ⇒ A matrix of constants which describes how the system changes between measurements

W ⇒ The random variable representing the randomness (noise) of the system between states, $W \sim N(\mu_w,Q) \sim R^n$.

One of the basic assumptions used by this thesis is that the precipitation storm cells are driven by a deterministic, non-random process. Therefore, the updated state matrix can be expressed as a time function of both

position and velocity in one dimension, and Equation 4.2 can be expressed mathematically as

$$\begin{bmatrix} X_{k+1} \\ Y_{k+1} \\ U_x \\ U_y \end{bmatrix} = \begin{bmatrix} 1 & 0 & T & 0 \\ 0 & 1 & 0 & T \\ 0 & 0 & 1 & 0 \\ 0 & 0 & 0 & 1 \end{bmatrix} \cdot \begin{bmatrix} X \\ Y \\ U_x \\ U_y \end{bmatrix} + \begin{bmatrix} W_X \\ W_Y \\ W_{U_x} \\ W_{U_y} \end{bmatrix} \quad . \quad (4.3)$$

3. Measurement model

The measurement model is used to update the state of the system after some additional information is obtained. This additional information is another set of location data from another radar presentation. Incorporated into the model is the randomness (noise) associated with the measurement. The system model for the Kalman filter process algorithm can be described mathematically as

$$Z = HX + V \quad , \quad (4.4)$$

where:

Z ⇒ The measured value, $Z \sim R^m$

H ⇒ The measurement matrix. It is assumed that all measurements are linearly related to the system state variable X by this matrix H

X ⇒ The present state vector

V ⇒ The random variable representing the randomness (noise) associated with the measurement Z,

$V \sim N(\mu_v, R) \sim R^m$.

Since the data obtained from the radar presentation only gives position data of the storm cell, there is no velocity component values to use in the measurement matrix. Therefore Equation 4.3 can be expressed mathematically as

$$\begin{bmatrix} X_{k+1}\ (long) \\ Y_{k+1}\ (lat) \\ 0 \\ 0 \end{bmatrix} = \begin{bmatrix} 1 & 0 & 0 & 0 \\ 0 & 1 & 0 & 0 \\ 0 & 0 & 0 & 0 \\ 0 & 0 & 0 & 0 \end{bmatrix} \cdot \begin{bmatrix} X \\ Y \\ U_x \\ U_y \end{bmatrix} + \begin{bmatrix} V_{long} \\ V_{lat} \\ 0 \\ 0 \end{bmatrix}. \qquad (4.5)$$

4. Kalman filter operation

The following summarizes the Kalman process analyzed in detail in References 10, 11, and 12. The Kalman filter obtains initial values from a radar images that includes the x- and y-position of the centroid of the storm cell. The user must input the initial mean (μ_o) and the covariance (σ_o^2) for the Kalman filter to initially use to perform its movement prediction algorithm. To update the mean and covariance the following equations are used,

$$(Mean) \rightarrow \mu = \phi\mu_o + \mu_w$$

$$(Covariance) \rightarrow \sigma^2 = \phi\sigma_o^2\phi^t + Q \qquad (4.6)$$

Then to update the estimated mean (μ) and the covariance (σ^2), the measurement step is performed using

$$K = \sigma_o^2 H^t \, (H\sigma_o^2 H^t + R)^{-1}$$

$$\mu = \mu_o + K(Z - \mu_v - H\mu) \qquad (4.7)$$

$$\sigma^2 = (I - KH)\,\sigma_o^2 \quad ,$$

where

K ⇒ The Kalman gain

H ⇒ The measurement matrix

H^t ⇒ The "transposed" measurement matrix

R ⇒ The covariance of the measurement noise

μ_v ⇒ The mean of the measurement noise

Z ⇒ The actual measurement

I ⇒ The identity matrix.

The only information, obtained from radar, when tracking the precipitation storm cells is its position data (x- and y-coordinates), the initial values estimated for the

state vector and the Q-matrix (mathematically derived and variables discussed in Reference 10 and variables inputs provided in Appendix C) are shown below:

$$\begin{bmatrix} x \\ y \\ 0 \\ 0 \end{bmatrix} \quad and \quad \begin{bmatrix} q11 & 0 & q12 & 0 \\ 0 & q11 & 0 & q12 \\ q12 & 0 & q22 & 0 \\ 0 & q21 & 0 & q22 \end{bmatrix} \qquad (4.8)$$

The algorithm incorporating the Kalman filter tracker was written using *386-Matlab*. The computer listing is provided in Appendix D.

C. ELLIPSE UNCERTAINTY MODEL

Because of the limited number of data points available for each storm cell a simple statistical mean value equation was used to approximate the shape and orientation of the *Image-Pro Plus* ellipse. This best fit statistical equation would be used to account for the ellipse growth/decay and orientation weighing value. The following equation was developed to

provide simple statistical representation the change of a storm cell's shape for each axis.

$$\left[\frac{\mu_{L_{axis}}}{t} \cdot \Delta t\right] * W_f \qquad (4.9)$$

where

μ_{Laxis} ⇒ The mean length change of the axis over a number of data point

t ⇒ The total time period the mean length change was calculated .

Δt ⇒ The incremental time change between the next data point

W_f ⇒ The statistical weighing function

V. DATA ANALYSIS OF STORM CELLS

Fifteen days of data were collected and examined for candidate precipitation cell tracking data. Ten cell data sets were selected for evaluation. These ten cases were turned into elliptical data format and their centroids were manually plotted in a time/position geographic format. From this information, trial runs on the Kalman tracking algorithm indicated that four of the data sets had such large variations that the Kalman would not be able to provide any useful output. These four cases are classified as non-successful implementation cases of the tracking algorithm. The remaining six cases are evaluated in detail. These six specific storm cell data sets were identified as candidate inputs to the newly developed motion model. Even over water, the storm cells appeared to make erratic (zigs), or abrupt course and speed changes, similar to an evasive submarine target. These abrupt changes are basically the result of:

- *Image-Pro Plus* ellipse generating mathematics.
- The fact that the radar intensity feature was not used to identify the "real" centroid of the storm cell.
- Multi-cell structure of the thunderstorm systems where a component of movement is due to new cell growth vice translation.

The main purpose of the Kalman filter tracking algorithm is to provide predictive tracking information on the storm

cells, and there is a need to be able to detect a cell's valid course and speed change to re-initialize the motion model. Previous research has documented the difficulty experienced when attempting to identify individual storm cells from a radar return [Ref. 13]. The figure below illustrates the complex structure of large precipitation storms. The presence of cell growth and decay in multi-cell storms makes the task of storm tracking more difficult.

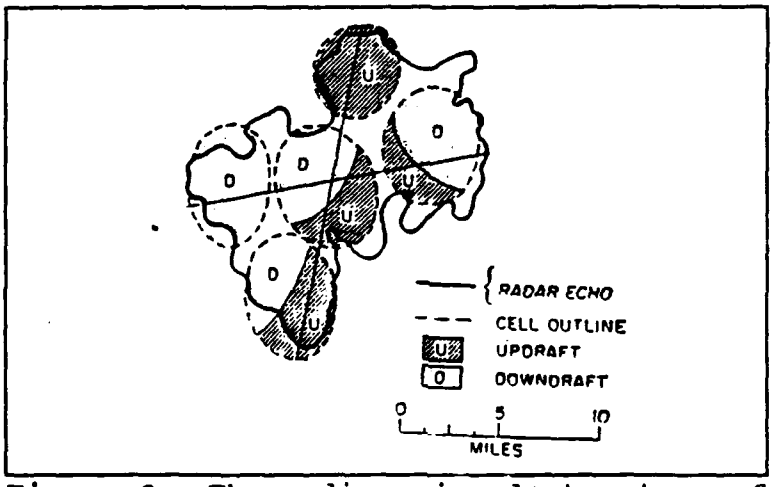

Figure 3. Three dimensional structure of a thunderstorm containing several cells [Ref. 13:p. 469].

The following sections contain the tracks of the storm cells selected to test the Kalman filter algorithm. All of the coordinates in the figures below have been normalized to non-dimensional *Image-Pro Plus* units. Each unit is approximately 240 meters.

A. CASE #1 (18 AUGUST 1991)

The #1 case storm cell track was very erratic and had several large velocity changes during the tracking period. There were three distinct direction changes and three distinct velocity changes (Figure 4).

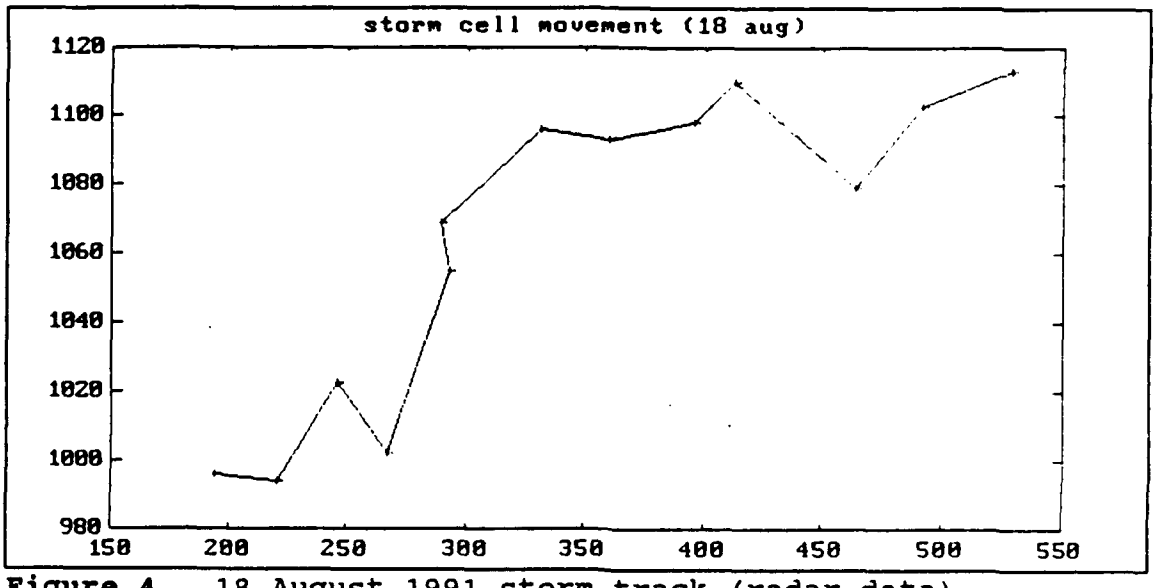

Figure 4. 18 August 1991 storm track (radar data).

The tracking algorithm was initiated using the first two, three, and four points of the storm data set (Figure 5). Because of the erratic movement of the cell the tracking algorithm is never able to accurately predict the centroid location. Refer to Appendix E tables for the actual centroid location prediction and the centroid error between the Kalman predicted and the radar determined position.

The growth/decay of the ellipse was approximated, using the first four points of data and the simple statistical algorithm in Equation 4.9:

$$L_{maj} = ((+0.27) \times \Delta t) \times 0.6$$

$$L_{min} = ((+0.26) \times \Delta t) \times 0.6$$

Refer to Appendix F and G tables for the calculated growth/decay values of the major/minor axes. The simple statistical algorithm was not adequate in predicting the actual growth. For this case only about 40% of the actual ellipse area were covered by the predicted ellipses. Therefore the results of this data set did not support the simple statistical algorithm to predict growth and decay.

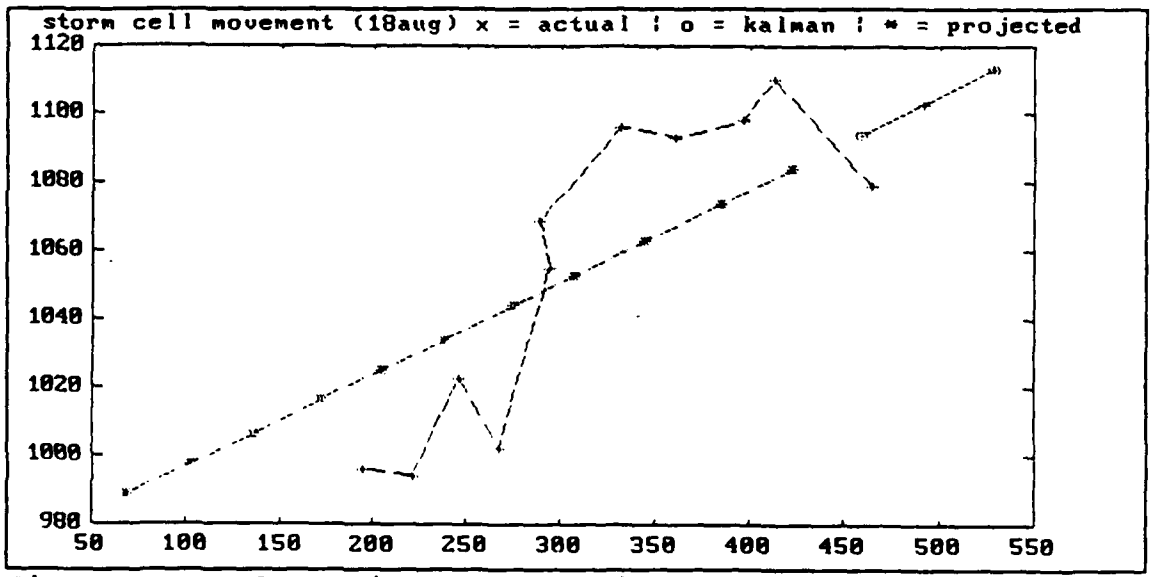

Figure 5. Kalman filter prediction for 18 August storm.

B. CASE #2 (31 AUGUST 1991)

The #2 case storm cell track was very erratic and had several large position jumps during the tracking period. There are three extreme direction changes and two distinct velocity changes during the cell data series (Figure 6).

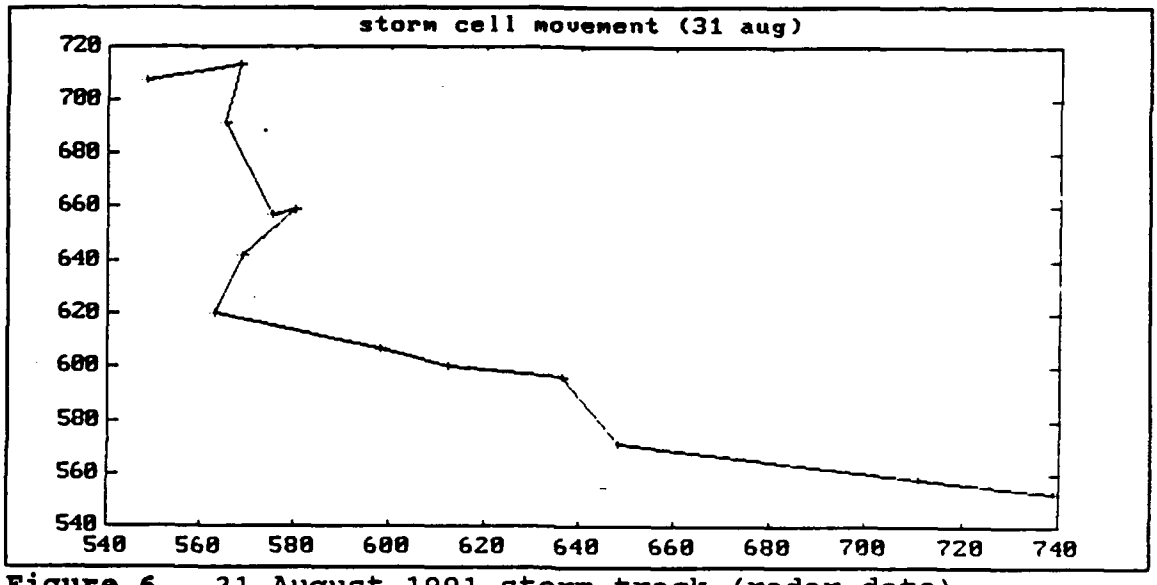

Figure 6. 31 August 1991 storm track (radar data).

Because of the erratic direction changes at the beginning of the data series, the tracking algorithm was initiated with points seven, eight, and nine (Figure 7). Refer to Appendix E tables for the actual centroid location prediction and the centroid error between the Kalman predicted and the radar determined position. The growth/decay of the ellipse was

approximated by the simple statistical algorithm in Equation 4.9:

$$L_{maj} = ((+0.69) \times \Delta t) \times 0.6$$

$$L_{min} = ((-0.01) \times \Delta t) \times 0.6$$

Refer to Appendix F and G tables for the calculated growth/decay values. The tracking program and simple statistical algorithm predicted the track and the actual growth for over 40 minutes. For this case over 80% of the actual ellipses were covered by the predicted ellipses. Therefore the results of this data series were considered a very good approximation of the actual radar data.

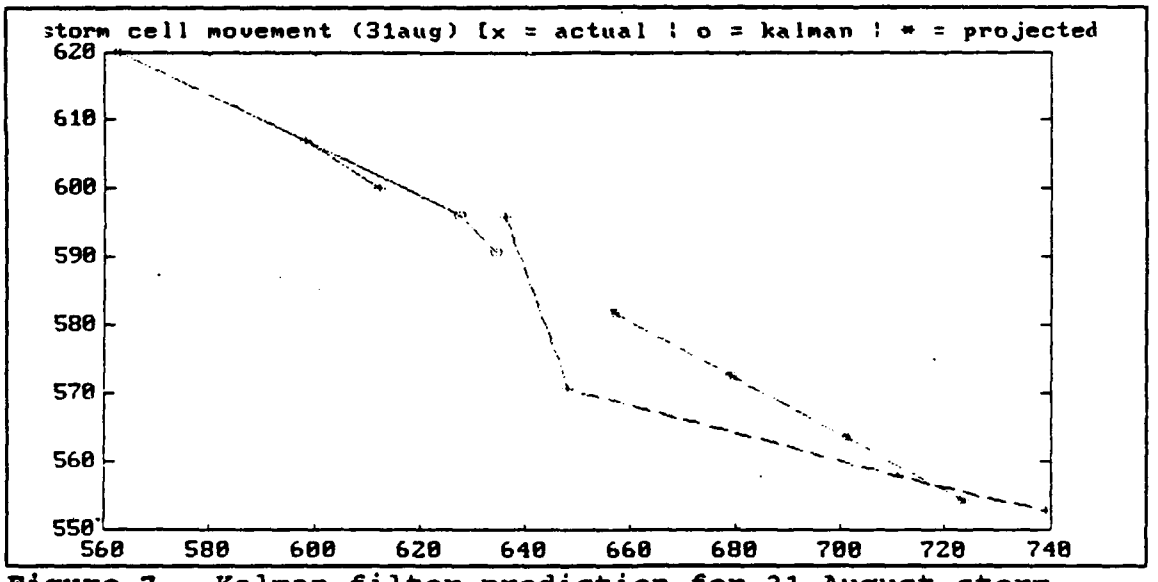

Figure 7. Kalman filter prediction for 31 August storm.

C. CASE #3 (10 SEPTEMBER 1991)

The #3 case storm cell track was also very erratic and had several large velocity changes during the tracking period. There are seven extreme direction changes and two distinct velocity changes (Figure 8).

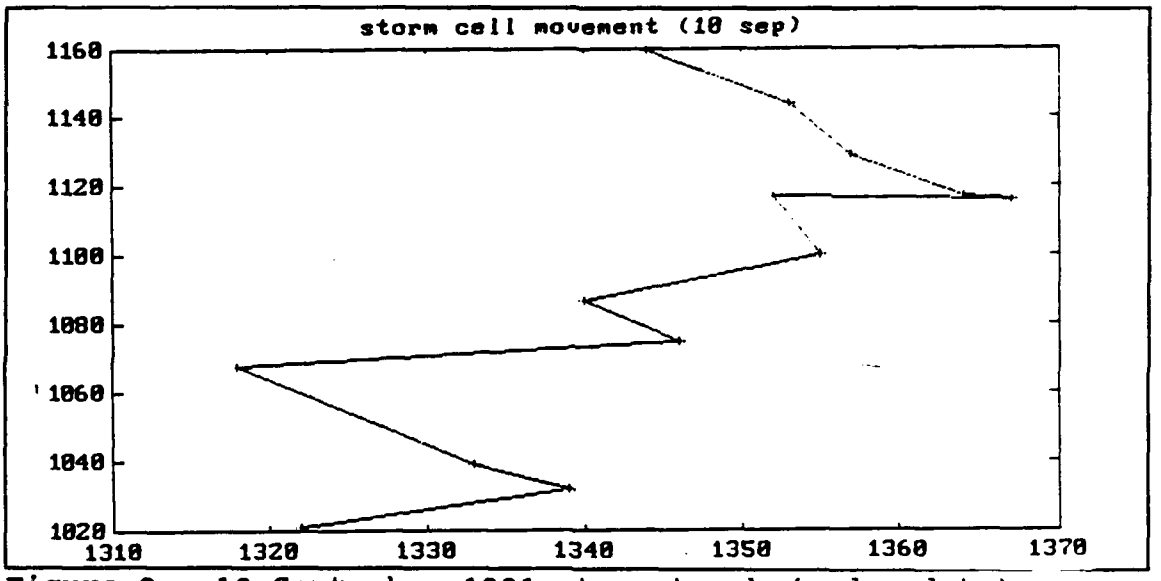

Figure 8. 10 September 1991 storm track (radar data).

The tracking algorithm was initialized with the first three points of the cell data, but because of an enormous direction change, the tracking system was restarted using the fifth, sixth, and seventh data points (Figure 9). Refer to Appendix E tables for the actual centroid location prediction and the centroid error between the Kalman predicted and the radar determined position. The growth/decay of the ellipse

was approximated by the simple statistical algorithm in Equation 4.9:

$$L_{maj} = ((-0.005) \times \Delta t) \times 0.6$$

$$L_{min} = ((-0.0253) \times \Delta t) \times 0.6$$

Refer to Appendix F and G tables for the calculated growth/decay values. The tracking program and simple statistical algorithm predicted the track and the actual growth for over 50 minutes. For this case over 70% of the actual ellipses were covered by the predicted ellipses. Therefore the results of this data series were considered a very good approximation of the actual radar data.

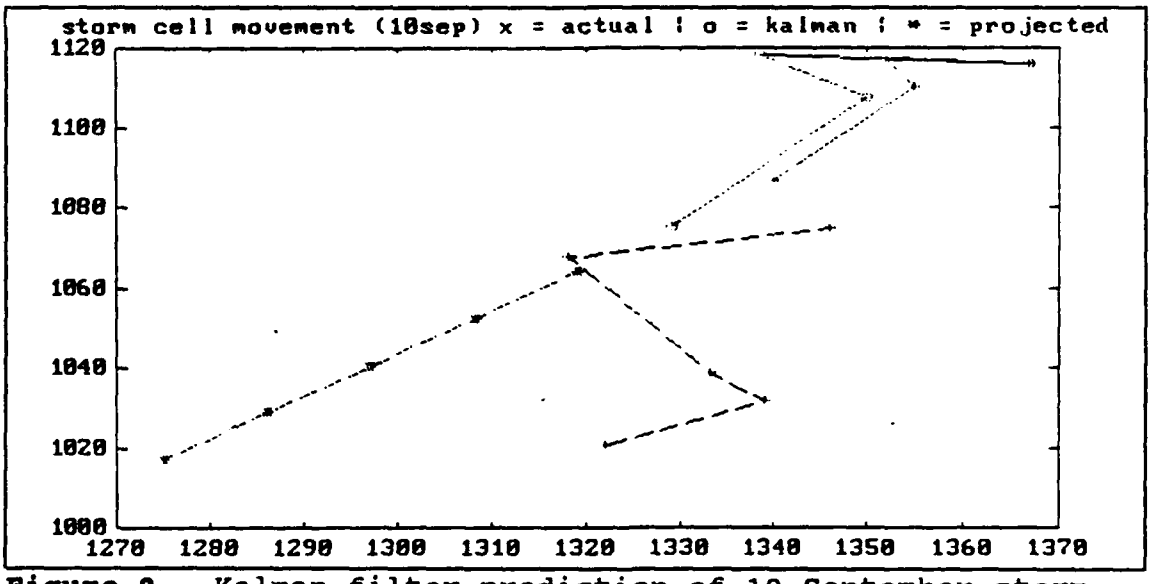

Figure 9. Kalman filter prediction of 10 September storm

D. CASE #4 (12 SEPTEMBER 1991)

The Kalman tracking algorithm was initialized with the first three data points (Figure 11). There are seven extreme course changes and two distinct speed changes (Figure 10). Refer to Appendix E tables for the actual centroid location prediction and the centroid error between the Kalman predicted and the radar determined position.

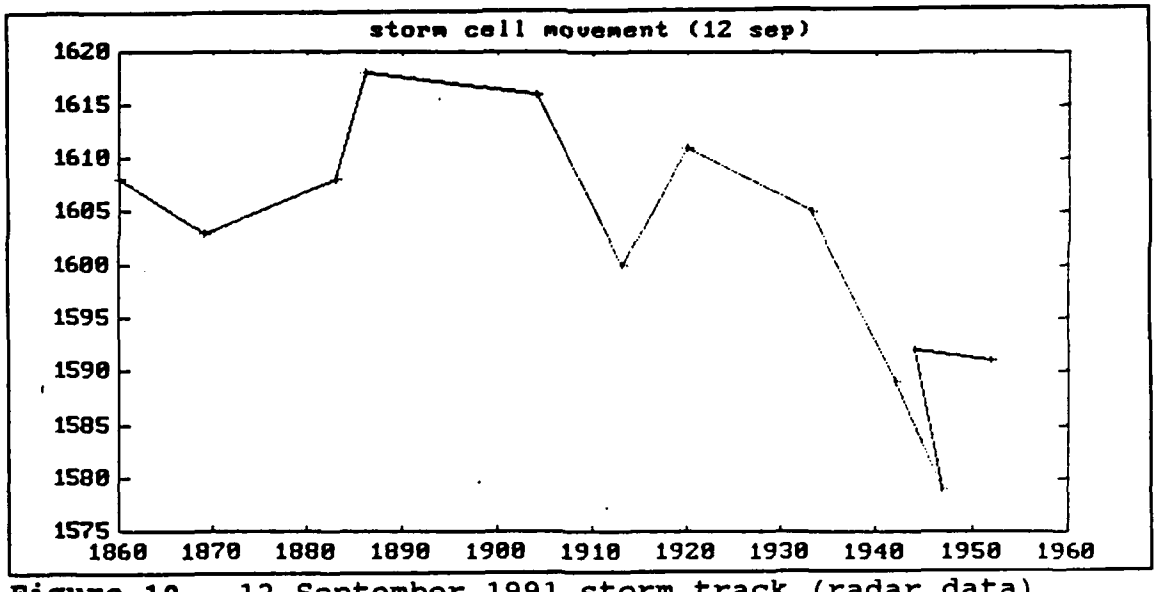

Figure 10. 12 September 1991 storm track (radar data)

The growth/decay of the ellipse was approximated by the simple statistical algorithm in Equation 4.9:

$$L_{maj} = ((+0.30) \times \Delta t) \times 0.6$$

$$L_{min} = ((-0.032) \times \Delta t) \times 0.6$$

Refer to Appendix F and G tables for the calculated growth/decay values. The tracking program and simple statistical algorithm predicted the actual track and the growth for over 40 minutes. For this case over 80% of the actual ellipses were covered by the predicted ellipses. Therefore the results of this data series were considered a very good approximation of the actual radar data.

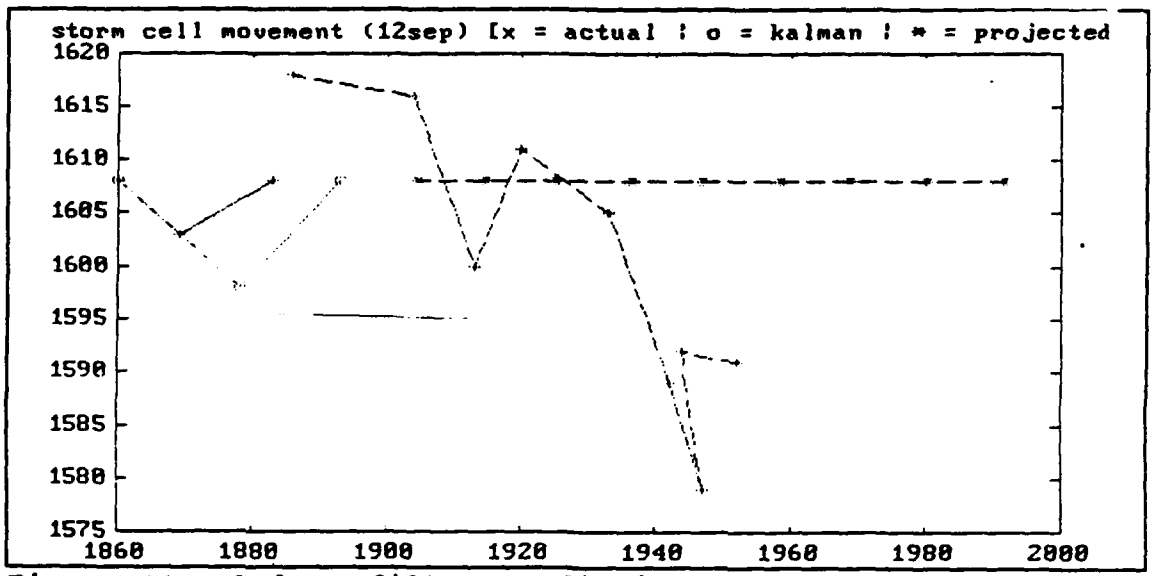

Figure 11. Kalman filter prediction for 12 September storm.

E. CASE #5 (14 SEPTEMBER 1991)

The tracking algorithm was initialized with the first three data points (Figures 12 and 13). Refer to Appendix E tables for the actual centroid location prediction and the

centroid error between the Kalman predicted and the radar determined position.

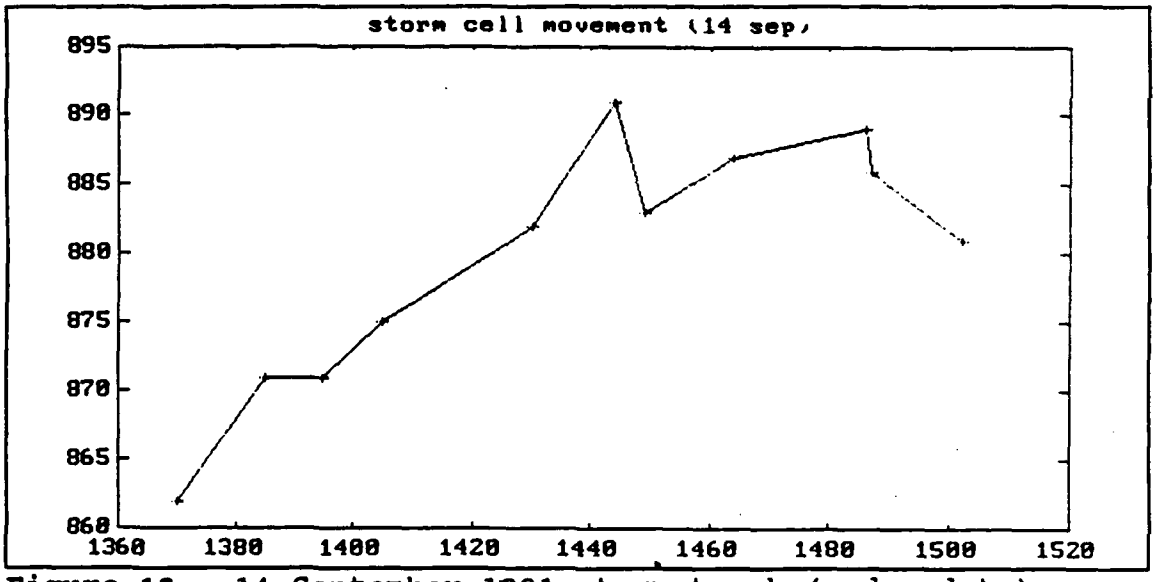

Figure 12. 14 September 1991 storm track (radar data).

The growth/decay of the ellipse was approximated by the simple statistical algorithm in Equation 4.9:

$$L_{maj} = ((+0.33) \times \Delta t) \times 0.6$$

$$L_{min} = ((-0.66) \times \Delta t) \times 0.6$$

Refer to Appendix F and G tables for the calculated growth/decay values. Both the Kalman and the cloud ellipses were very large. The tracking program and simple statistical algorithm was adequate in predicting the actual growth for over 40 minutes. Over 90% of the actual ellipses were covered by the predicted ellipses. Therefore the results of this data

series were considered an excellent approximation of the actual radar data.

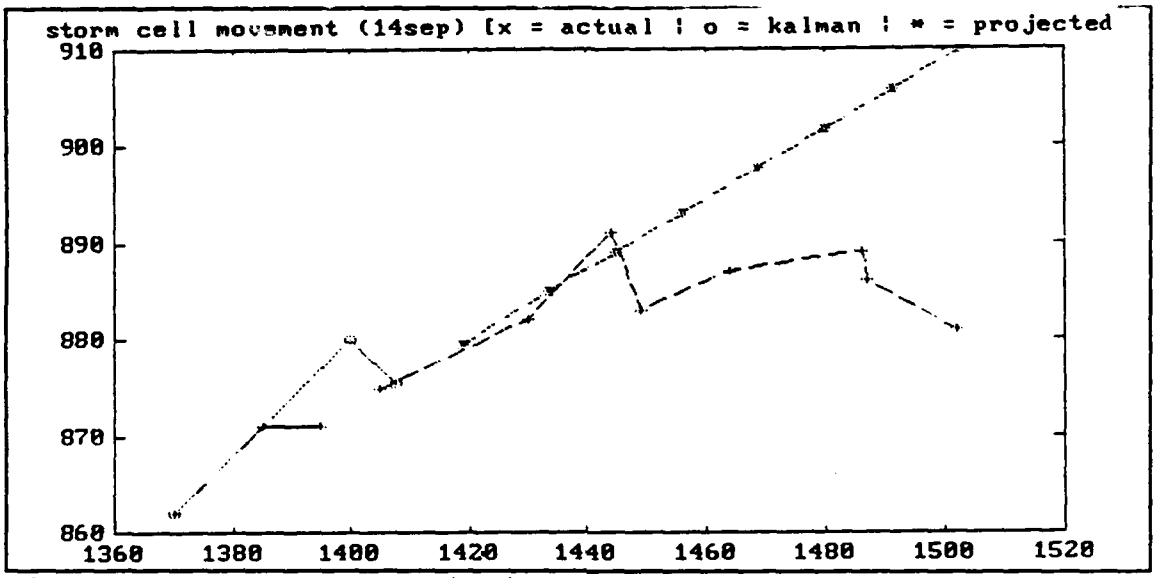

Figure 13. Kalman prediction of 14 September storm data.

F. CASE #6 (02 OCTOBER 1991)

The 02 October storm was the most well behaved storm cell tracked during the data collection period. There were no erratic course changes and the data set contained only one rather large velocity change (Figure 14). The tracking algorithm was initiated using the two, three, and four points of the storm data set (Figure 15). Refer to Appendix E tables for the actual centroid location prediction and the centroid

error between the Kalman predicted and the radar determined position.

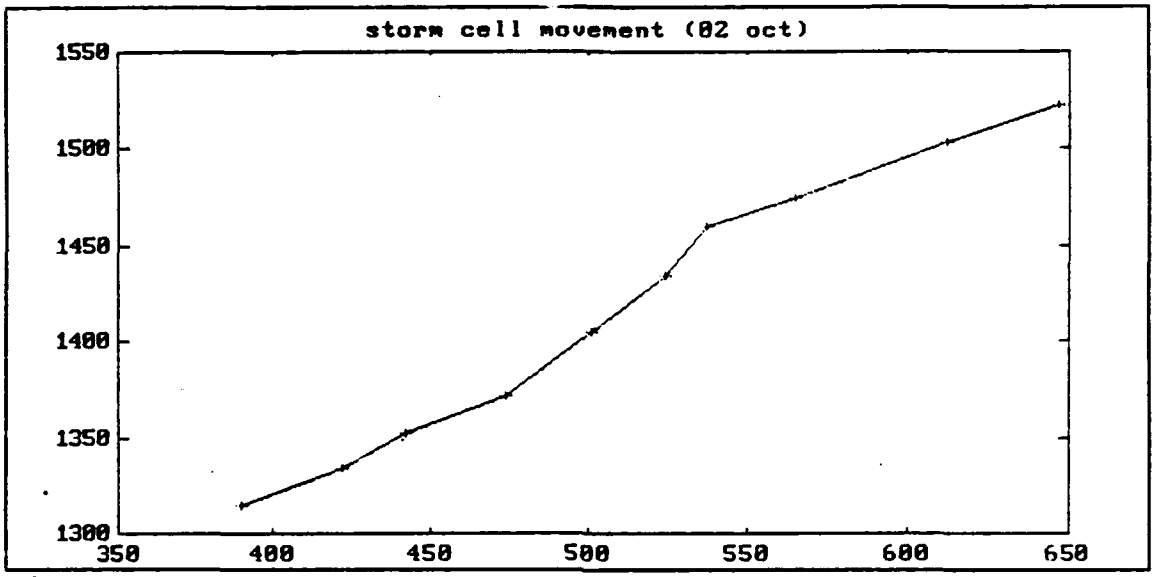

Figure 14. 02 October 1991 storm track (radar data).

The growth/decay of the ellipse was approximated by the simple statistical algorithm in Equation 4.9:

$$L_{maj} = ((+0.037) \times \Delta t) \times 0.6$$

$$L_{min} = ((-0.048) \times \Delta t) \times 0.6$$

Refer to Appendix F and G tables for the calculated growth/decay values. Both the Kalman and the cloud ellipses were very large. The tracking program and simple statistical algorithm was adequate in predicting the actual growth for over one and a half hours. Over 75% of the actual ellipses were covered by the predicted ellipses. Because of the well

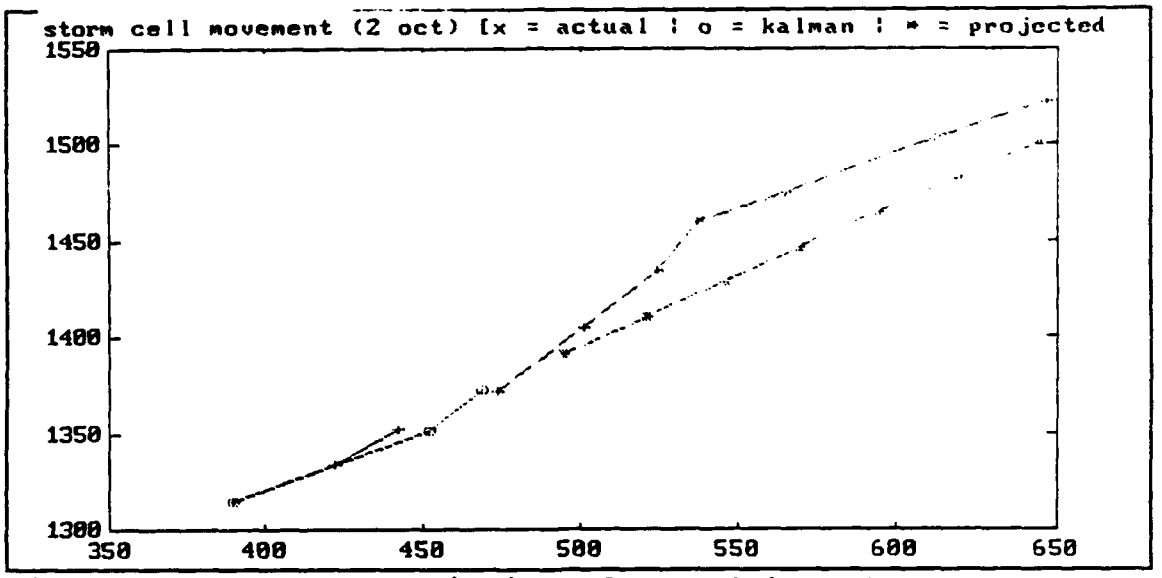

Figure 15. Kalman prediction of 02 October storm.

behaved tracking agreement for this storm cell, the disappointment for the case was in not having better ellipse area coverage. Therefore more effort needs to be made in refining the statistic growth/decay factor model and establishing a better weighing factor.

G. DATA ANALYSIS SUMMARY

Overall from the ten cases selected for the trial and six cases selected for evaluation, five cases provided successful results. An examination of the Kalman tracker predictions and the storm cell's radar position reveal a mean prediction centroid error for 30 minute predictions of approximately 5.81 km with a standard deviation of 3.64 km. These successes would indicate the value of further examination of a

Kalman/statistical algorithm as a means to track precipitation storm cells for short term positional forecasts.

VI. CONCLUSIONS AND RECOMMENDATION FOR FURTHER STUDY

A. CONCLUSIONS

The short term forecasting capability of the Kalman filter tracking algorithm could be evaluated in six of ten storm cells tracked by the radar. The inherently short life span of normal precipitation cells, as previously mentioned, does not allow for full appreciation of the Kalman filter effectiveness. The basic premise that precipitation storm cells behave in a predictable manner over periods of time that can be tracked with a Kalman filter has not been proven to be true in the strictest statistical sense. The results indicated that storm cells tracks can be predicted, with approximately 70% accuracy, for 30-50 minutes. There are several assumptions for the limited success of the Kalman tracking algorithm:

- Use of radar intensity to locate the cell center was not used.
- Limited time window for data collection of the storm cells.
- Limited available equipment required significant time for conversion of the analog radar picture into a digitized data set.
- *Image-Pro Plus* software not optimal for storm cell elliptical centroid approximations.

- Perceived movement by the Kalman tracker could be new growth of the storm cell vice actual movement of the cell's centroid.
- The local dynamics of wind / sea surface temp and local pressure changes were not modelled into the Kalman tracking matrices.

Only the binary digital images were used with no intensity information because of a lack of available technical equipment. If intensity levels in the storm cell were detectable this may have allowed a more effective track to be evaluated as the highest intensity return usually is located near the centroid of the cell. This detection ability should reduce much of the abrupt and erratic input data which caused significant problems in handling the data in this thesis.

A limited time window was given by Kavouras for storm cell data collection. The two hour window restriction for cell tracking was required because of operational commitments for the Kavouras radar services. A longer access window to the Kavouras radar data should be obtained, or a dedicated Doppler radar platform (such as a naval vessel), to ensure that storm cells are tracked from their creation until they mature and finally die out. Further research must be completed in order to collect the necessary data to statistically verify the findings of this thesis. The short time period that Kavouras data was available did not consistently show the entire life of a storm cell. This could explain the erratic tracks observed on several data storm tracks.

The lack of available technical equipment capable of detect intensity information has already been discussed. A system needs to exist to transfer the radar images from the RADAC system to the image analysis computer. Presently the digitized data sets of the radar images required extensive off-line conversion time. The analog picture of the radar data was digitized using a Hewlett Packard Scanjet Plus. This was the only means of converting the radar data into a useable medium for the scientific image analysis software. Although strict procedures were developed to ensure no bias was introduced by this conversion procedure, the possibility of introducing error into the digitized data set cannot be completely ignored.

Image-Pro Plus software, though very powerful for many image analysis purposes, mistakenly merged the tracks of maturing storm cells with new developing cells. This resulted in the appearance of erratic direction and velocity for the cells. The ability to manipulate real-time data on video displays could have averted this cross-correlation and avoided the resultant very erratic course (zig) for the storm cell. The ellipse algorithm used to approximate irregularly shaped images does not appear to be effective in modelling the storm cell detected by radar. The software should make use of some type of weighing function when developing the elliptical shape to ensure the center of the cell is located at the point of the highest intensity return. Presently the algorithm uses

the radar return image to generate an ellipse around the cell, and then it does not include the entire cloud cell in the ellipse. The ellipse algorithm equalizes the amount of space (non-radar return) inside the ellipse with the amount of the cloud cell outside the ellipse.

The new cell generation is a problem for a non real-time radar analysis. Manual analysis can not determine whether a storm cell erratically changed course and speed in between data collection interval or whether a new storm cell was created by the maturing of an old storm. It was found impossible to differentiate storm cell centroid movement from new growth along the edge of the cell. Further investigation is required to determine if factors such as changes in wind speed/direction, pressure changes, local temperature changes can be used to identify possible changes in cell course/speed and area of extent. One area that was overlooked and needs to be investigated is the effect the Gulf stream has on the precipitation cell's movement.

Although originally it was felt that the Kalman filter could model the track of storm cells (over water) by constantly updating the mean movement and the error covariance matrix without intensive meteorological alterations. This was found not to be the case for the limited data collected. The vertical dynamics of the cell, source of the cell, and local wind/sea surface temp/pressure changes all may need to be included in the weighing functions of the tracking algorithm.

Overall the use of a Kalman tracking model to determine the position and probability of size of rain cells can be used successfully for short periods. Only one of the six best data sets provided a successful tracking for more than a one hour period. However Kalman was successful in accurately tracking 50% of the cases for 30 to 50 minutes. During these periods the predicted tracking ellipse contained more than 70% of the actual measured storm cell for 30 to 50 minutes of samples beyond the initial 18 to 20 minutes of input data.

Further research must be undertaken to make this Kalman movement model effective for tactical use. It would appear that simple positional input into the motion model will not be enough to predict where a storm cell will track over a period of a few hours. It is believed that critical meteorological parameters influencing the motion of storm cells can be statistically defined and incorporated into the Kalman filter error covariance matrix. The more accurately all the forces acting on the storm cells can be included in the tracking algorithm, the more effective the tracker is in predicting the storm's future position.

B. RECOMMENDATION FOR FURTHER STUDY

Follow-on research to incorporate a "gating-function" in the Kalman algorithm, to readily identify erratic position, data zigs or the development of new cells, is required. A mathematical function could be set up to accept only those

data points (positional and meteorological) which fall within 2σ to 3σ of the mean values and discard those falling outside the "gate". This would optimize the tracking program to prevent the cross-correlation of dying cell tracks with new cell tracks nearby, preventing obviously erroneous course change being calculated by the tracker.

Identifying a real-time or near real-time tracking system that can produce digitized data sets is essential. The sooner the operator can identify a new cell development or a known cell's course change, the more effective the Kalman tracking algorithm can be. Actual real-time analysis is far more accurate than post analysis assumptions.

Follow-on research into the weighing of meteorological observations into the Kalman filter error covariance matrix algorithm should be explored. This could more accurately model how the cell's dynamics effect its movement.

APPENDIX A: RADAC WEATHER RADAR SYSTEM OPERATION

A. THE RADAC WEATHER RADAR COMPONENTS

The RADAC weather radar system supports the Naval Postgraduate School Meteorological Department's Synoptic Laboratory.

The RADAC weather radar system makes use of many remote radar sites, operated and maintained by the National Weather Service. The radar system transfers its imagery data to users via dedicated data-grade phone lines [Ref. 14]. Most of the remote sites use the WSR-57 radar system, which capabilities are described in Table II.

Table II WSR-57 RADAR SYSTEM CAPABILITY [REF. 14].

		WSR-57
Radar Band		S
Radar Frequency		1500 - 3900 MHz
Signal Wavelength		20.0 cm - 7.7 cm
Pulse Length	long	4 μsec @ 1200 m
	short	0.5 μsec @ 150 m
Range Resolution	long	600 m
	short	75 m
Beam Width (Approx.)	Degrees	2.0
	100 km	3490 m
	200 km	6980 m

The antenna assembly is of paraboloid design with a diameter of 3.658 meters. The figure below is the WSR-57 antenna assembly:

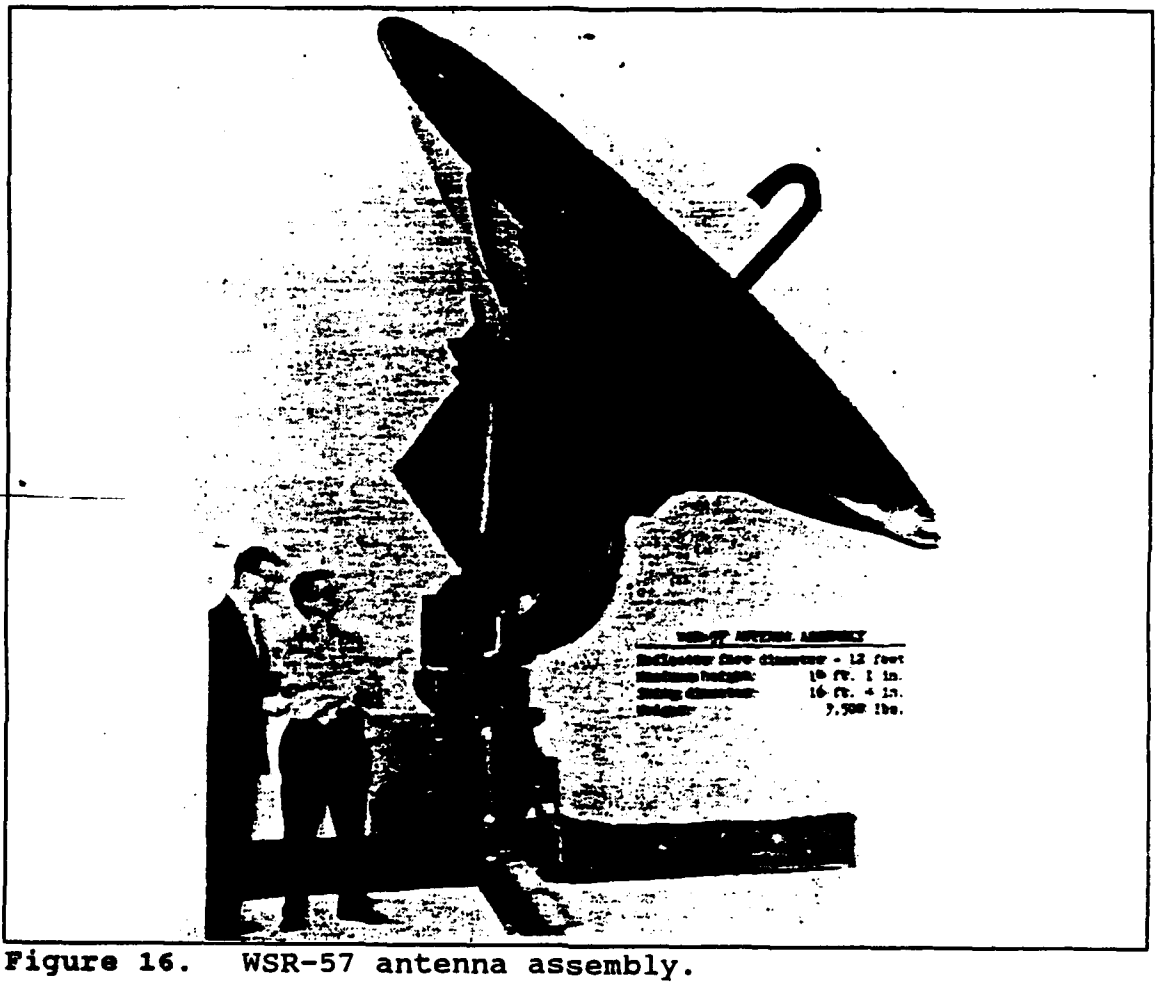

Figure 16. WSR-57 antenna assembly.

B. THE KAVOURAS (MODEL 1000) RADAC RECEIVER OPERATION

The Kavouras Model 1000 RADAC receiver is designed to enable remote display of precipitation storm echoes. The Model 1000 receives the radar data via a normal voice-grade telephone line. The receiver provides the user the ability of displaying the remote radar weather echoes, using various display formats. The RADAC receiver has the capability of displaying: four range setting (60, 120, 180, and 240 nautical miles), six precipitation levels (light, moderate,heavy, very heavy, intense, and extreme), and various time intervals (intervals from 3 to 27 minutes).

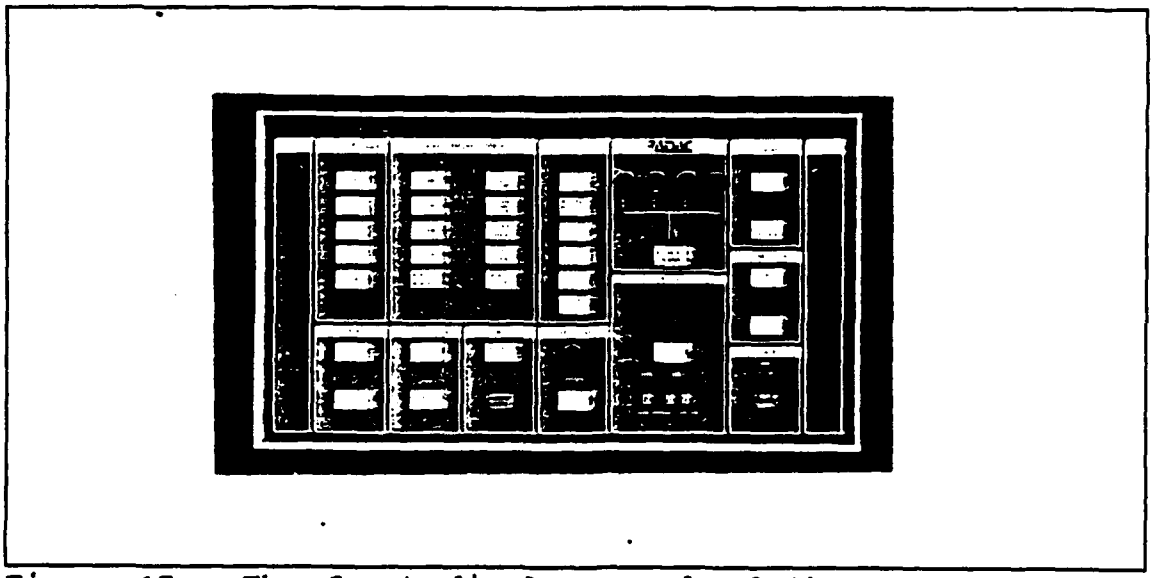

Figure 17. The front display panel of the Kavouras model 1000 RADAC receiver.

1. **Range selection switches**

The RADAC weather system display has the ability of presenting the user four radar ranges (60, 120, 180, and 240 nm). Because of the range attenuation limitations discussed below, the effective range of a WSR-57 is about 125 nm. Within this range the STC corrects for range attenuation. Though intense storms will show up out to 240 nm, the exact position may not be displayed reliably. The storm data used for this thesis was taken using the 120 nm range setting. The figure below shows the display of the range selection panel of the RADAC receiver.

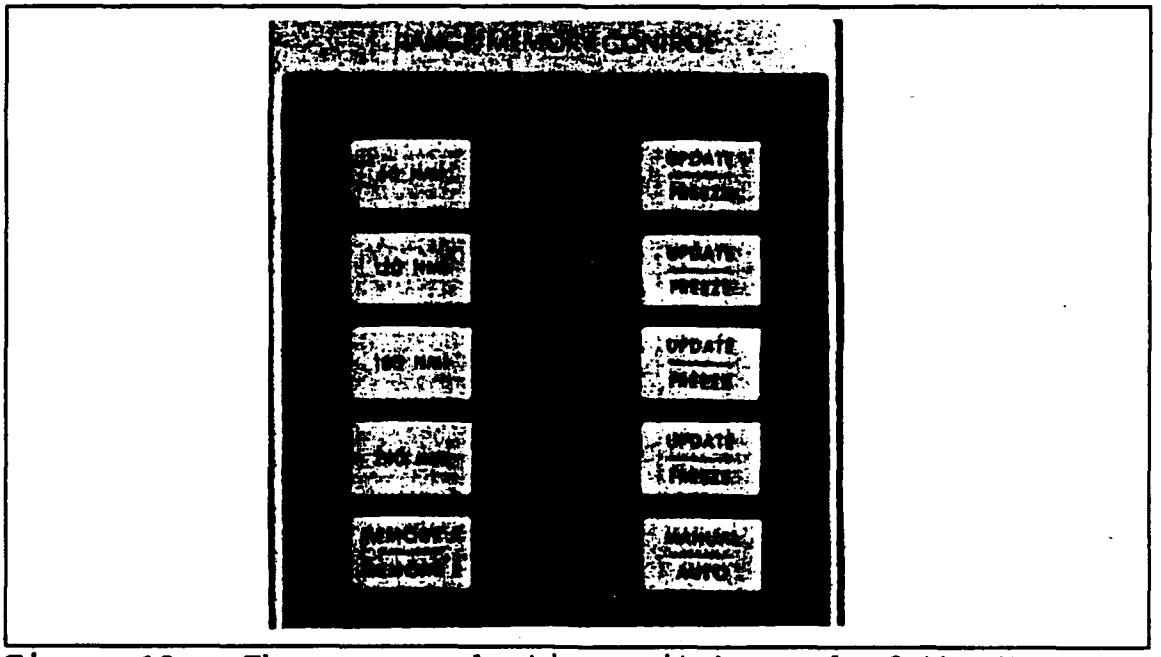

Figure 18. The range selection switch panel of the Kavouras model 1000 RADAC receiver.

2. Precipitation level switches

The RADAC weather system display has the ability of presenting the user six precipitation levels (light, moderate, heavy, very heavy, intense, and extreme).

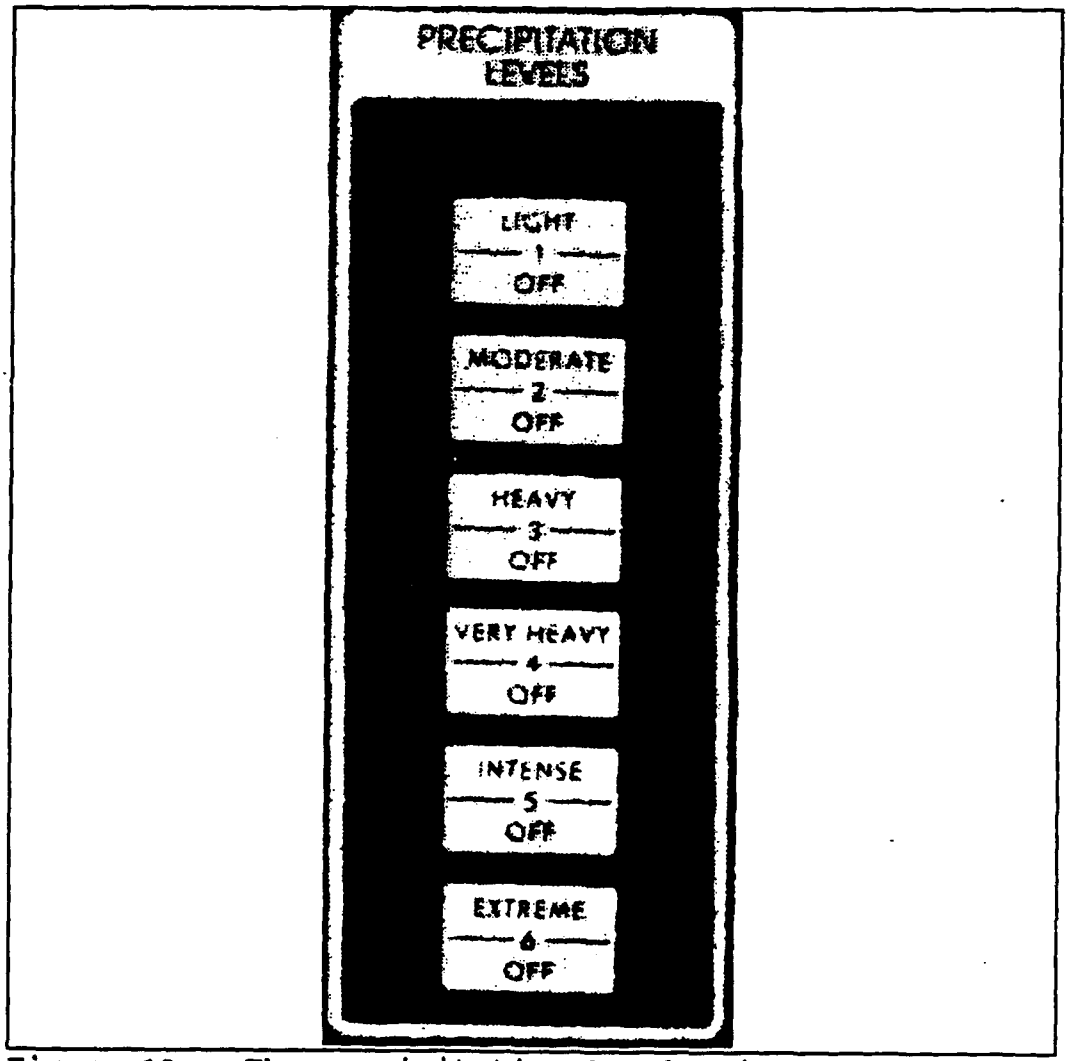

Figure 19. The precipitation level switch panel of the Kavouras model 1000 RADAC receiver.

These precipitation settings control the storm magnitude color display. These settings correspond to different precipitation rates as shown in the Table III.

Table III PRECIPITATION LEVEL, INTENSITY, AND RAINFALL RATES OF THE KAVOURAS MODEL 1000 RADAC RECEIVER [REF. 14].

Precipitation Level Switch Position	Intensity	Rainfall Rate (inches / hour)
1	Light	0.0 - 0.2
2	Moderate	0.2 - 1.1
3	Heavy	1.1 - 2.2
4	Very Heavy	2.2 - 4.5
5	Intense	4.5 - 7.1
6	Extreme	> 7.1

3. Time lapse storm switches

The time lapse feature allows the receiver to automatically receive and store a sequence of weather radar pictures. The RADAC Model 1000 receiver can store up to sixteen different images. The time sequence intervals can be selected from 3 - 27 minutes. This option was used in this thesis to collect the storm cell track data used to validate the tracking algorithm.

APPENDIX B: RADAC AND NODDS OUTPUT OF STORM CELL DATA

The following RADAC and NODDS storm cell data series were used for the tracking evaluation.

A. CASE #1 (18 August 1991)

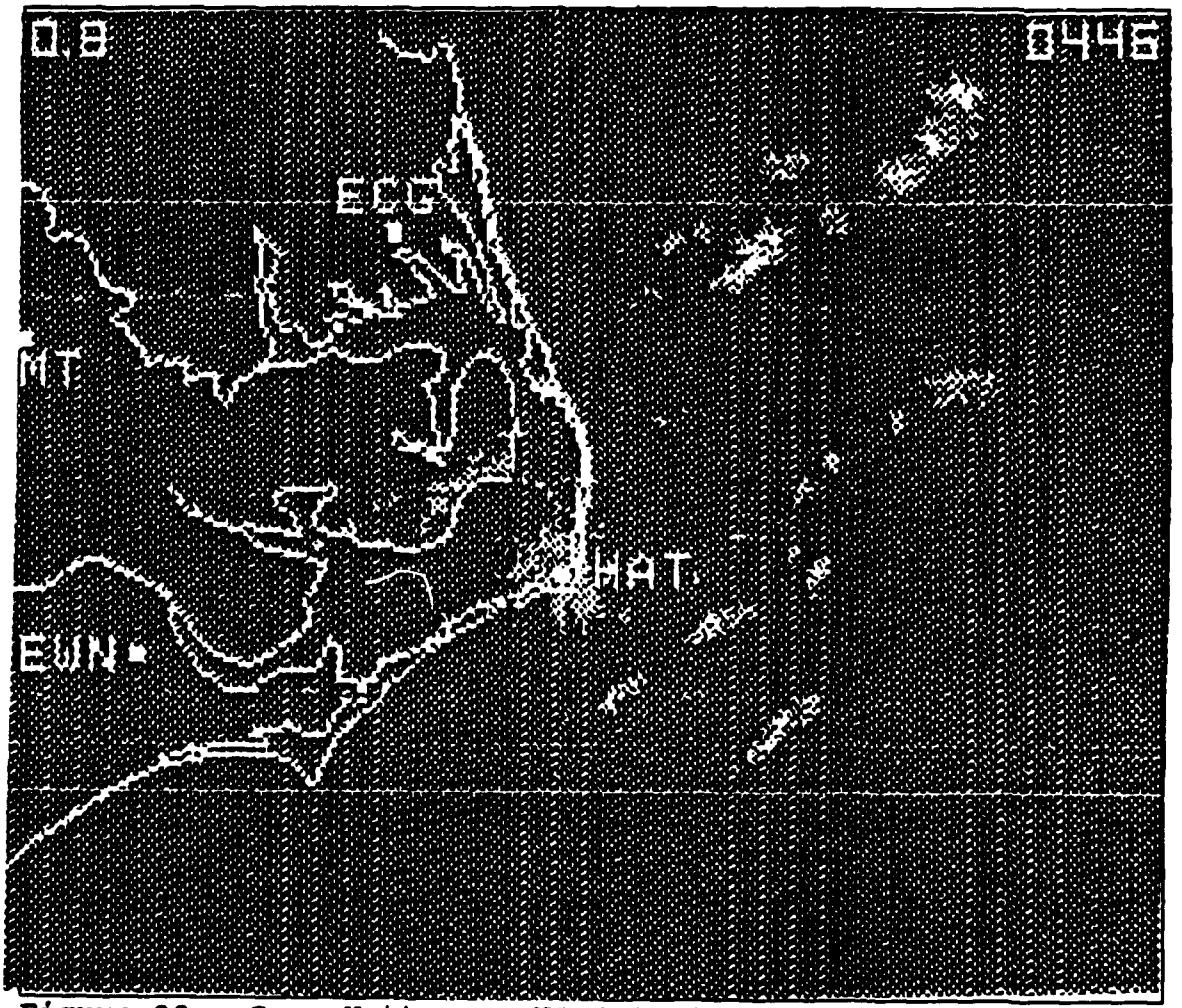

Figure 20. Cape Hatteras, NC (180446Z-180630Z AUG 91).

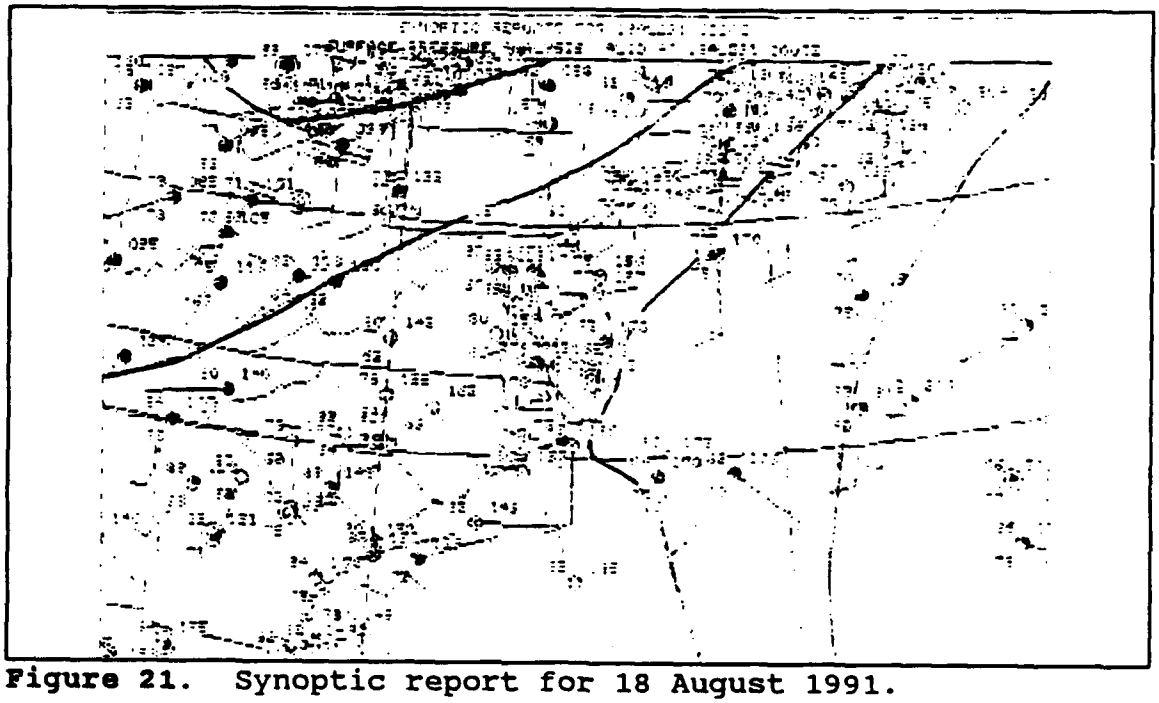

Figure 21. Synoptic report for 18 August 1991.

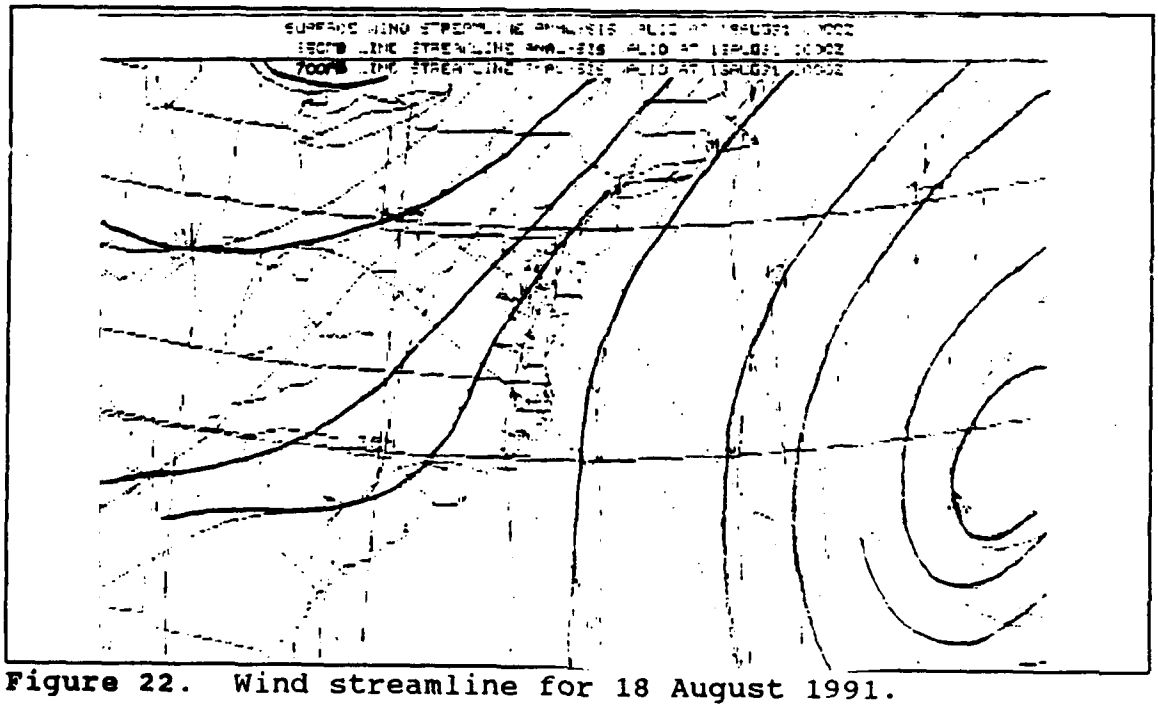

Figure 22. Wind streamline for 18 August 1991.

B. CASE #2 (31 August 1991)

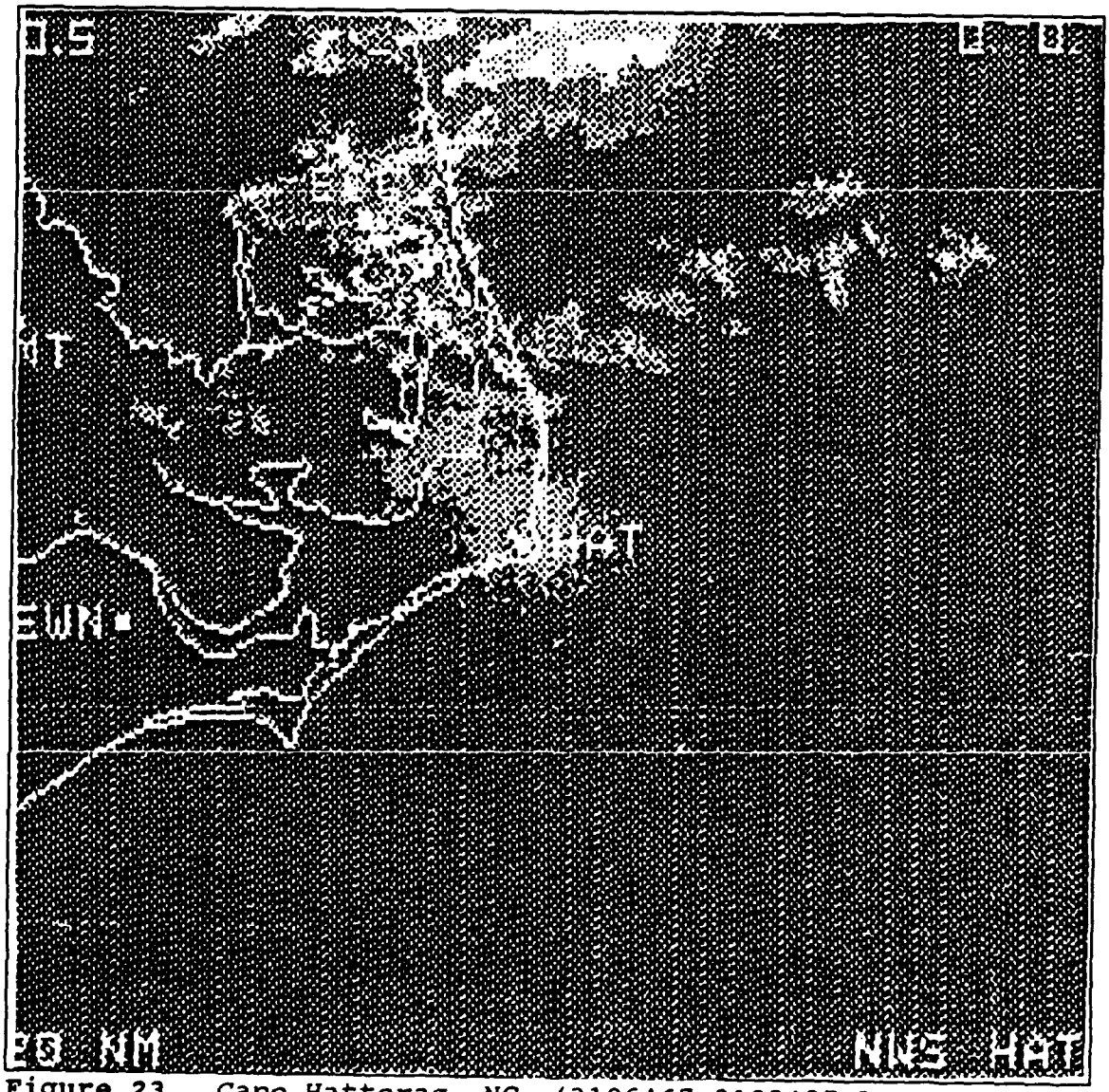

Figure 23. Cape Hatteras, NC (310646Z-310848Z August 1991).

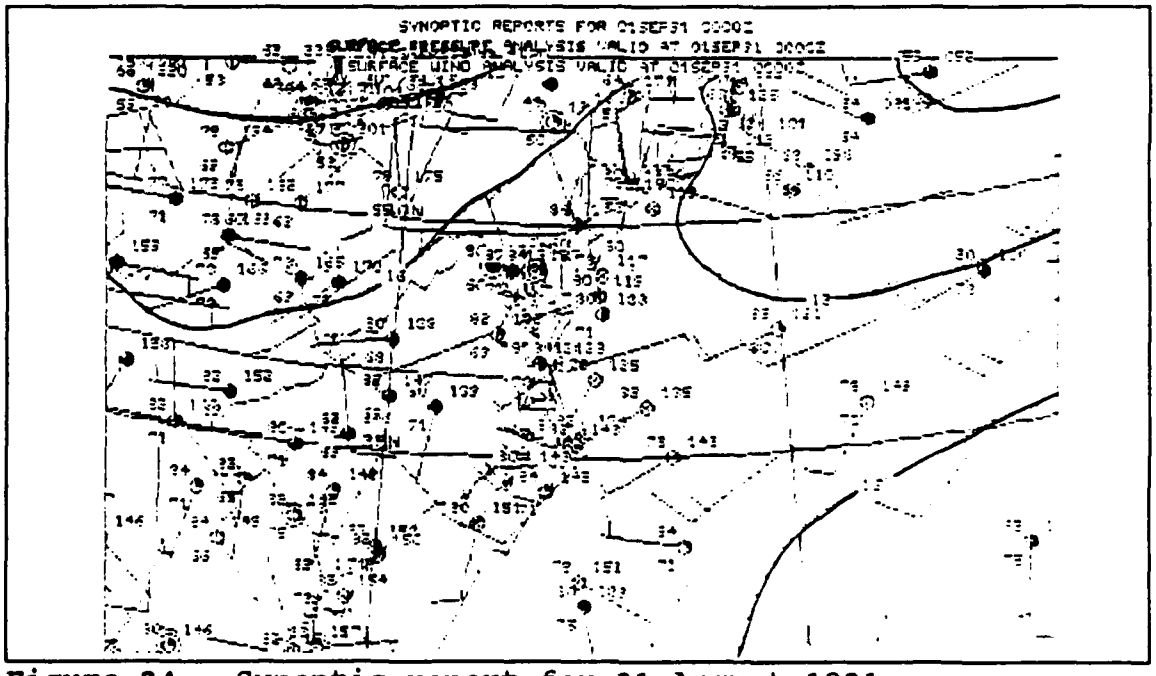

Figure 24. Synoptic report for 31 August 1991.

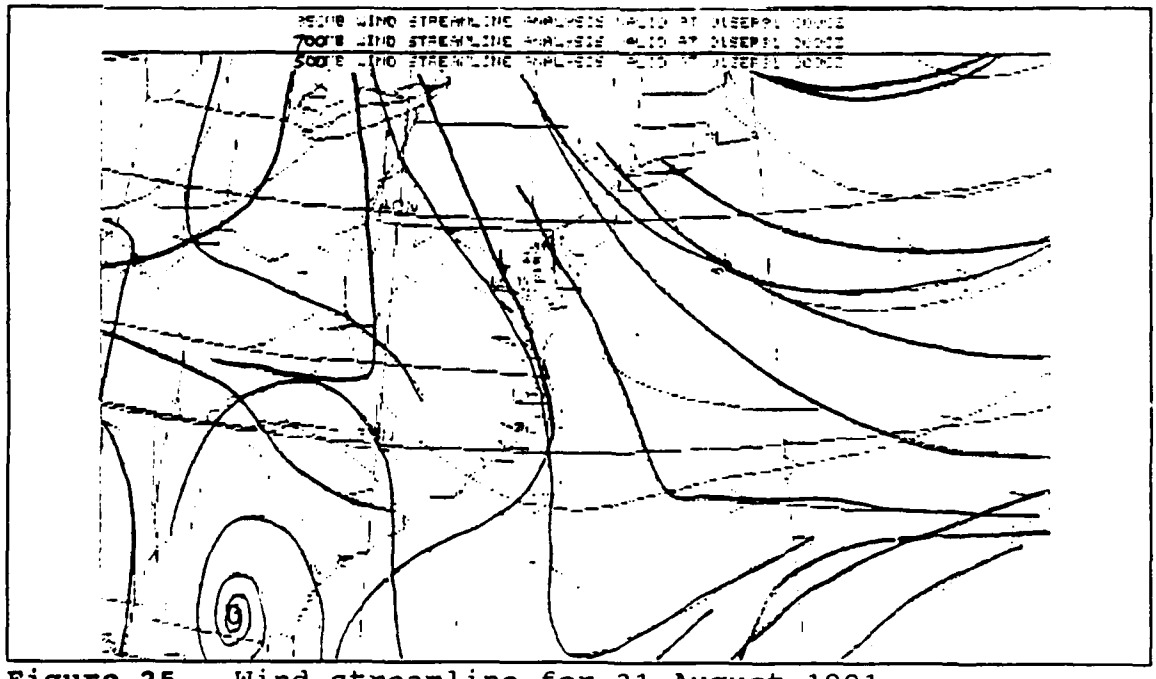

Figure 25. Wind streamline for 31 August 1991.

C. CASE #3 (10 September 1991)

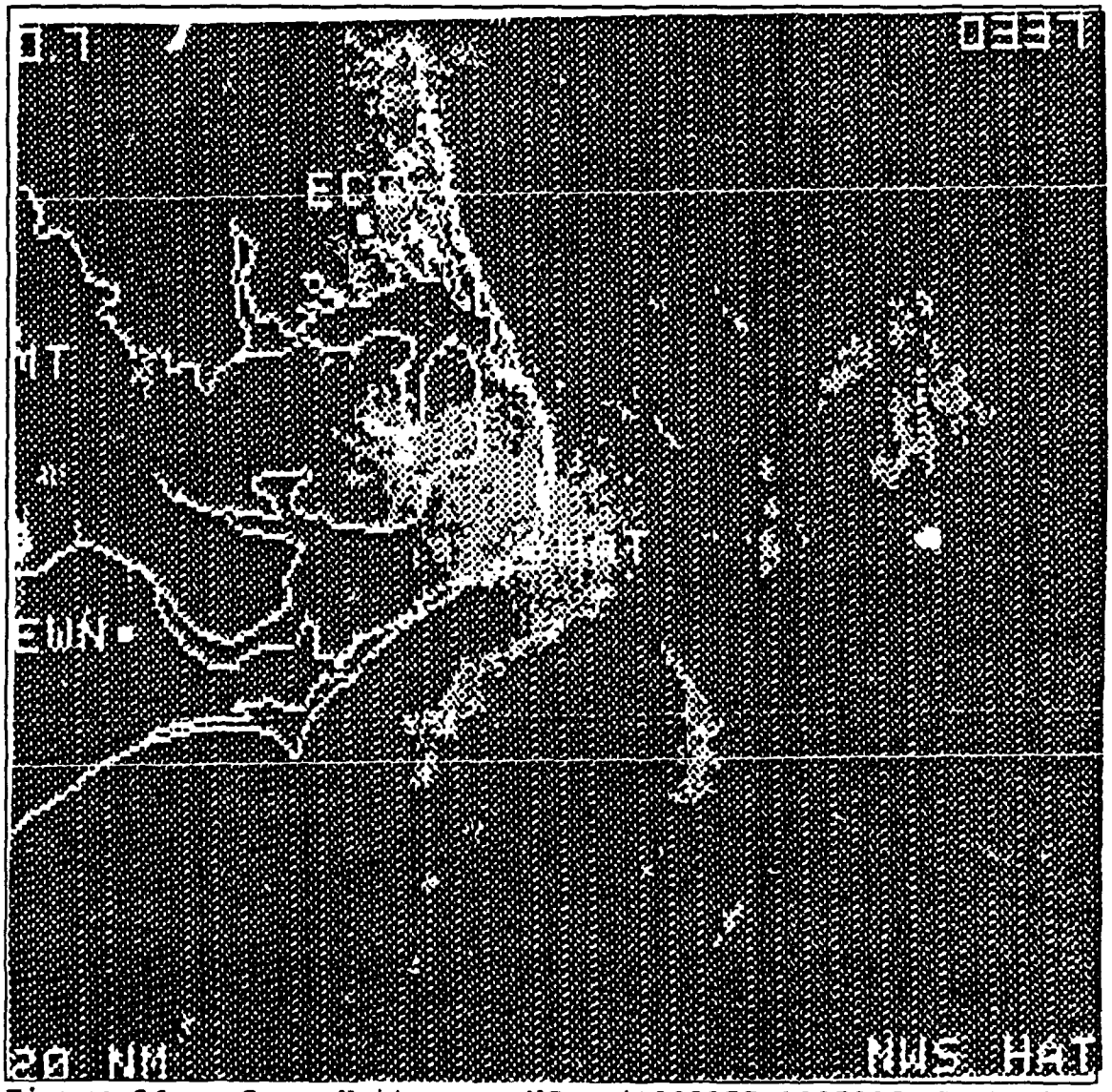

Figure 26. Cape Hatteras, NC (100337Z-100538Z September 1991).

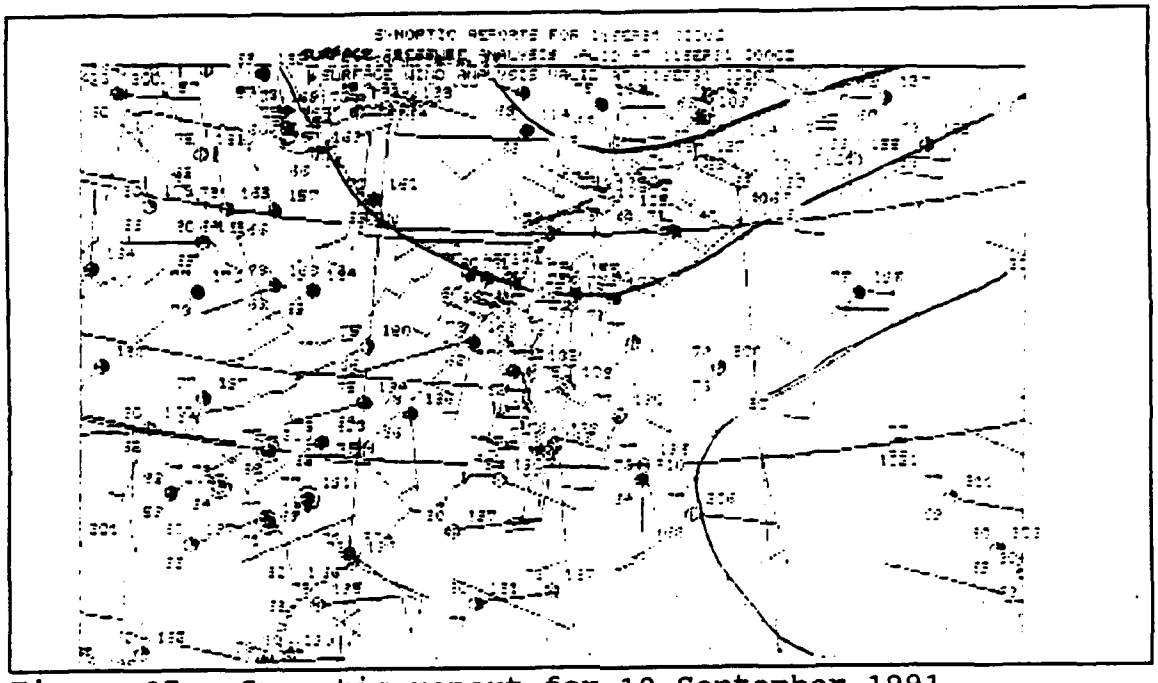

Figure 27. Synoptic report for 10 September 1991.

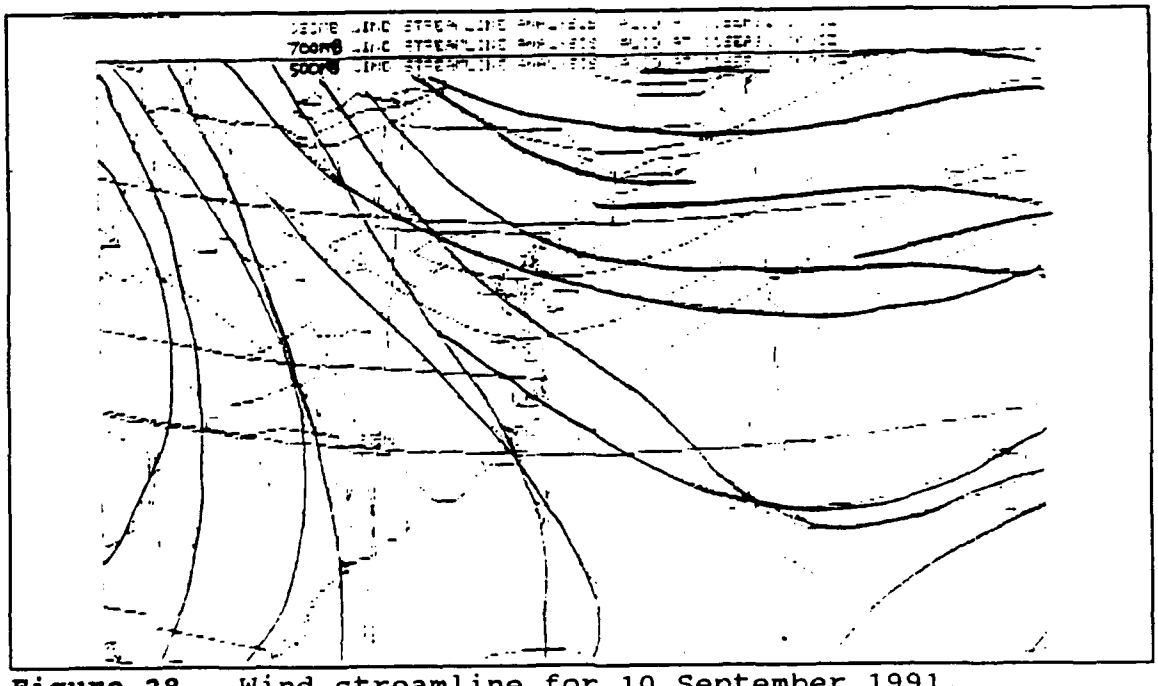

Figure 28. Wind streamline for 10 September 1991.

D. CASE #4 (12 September 1991)

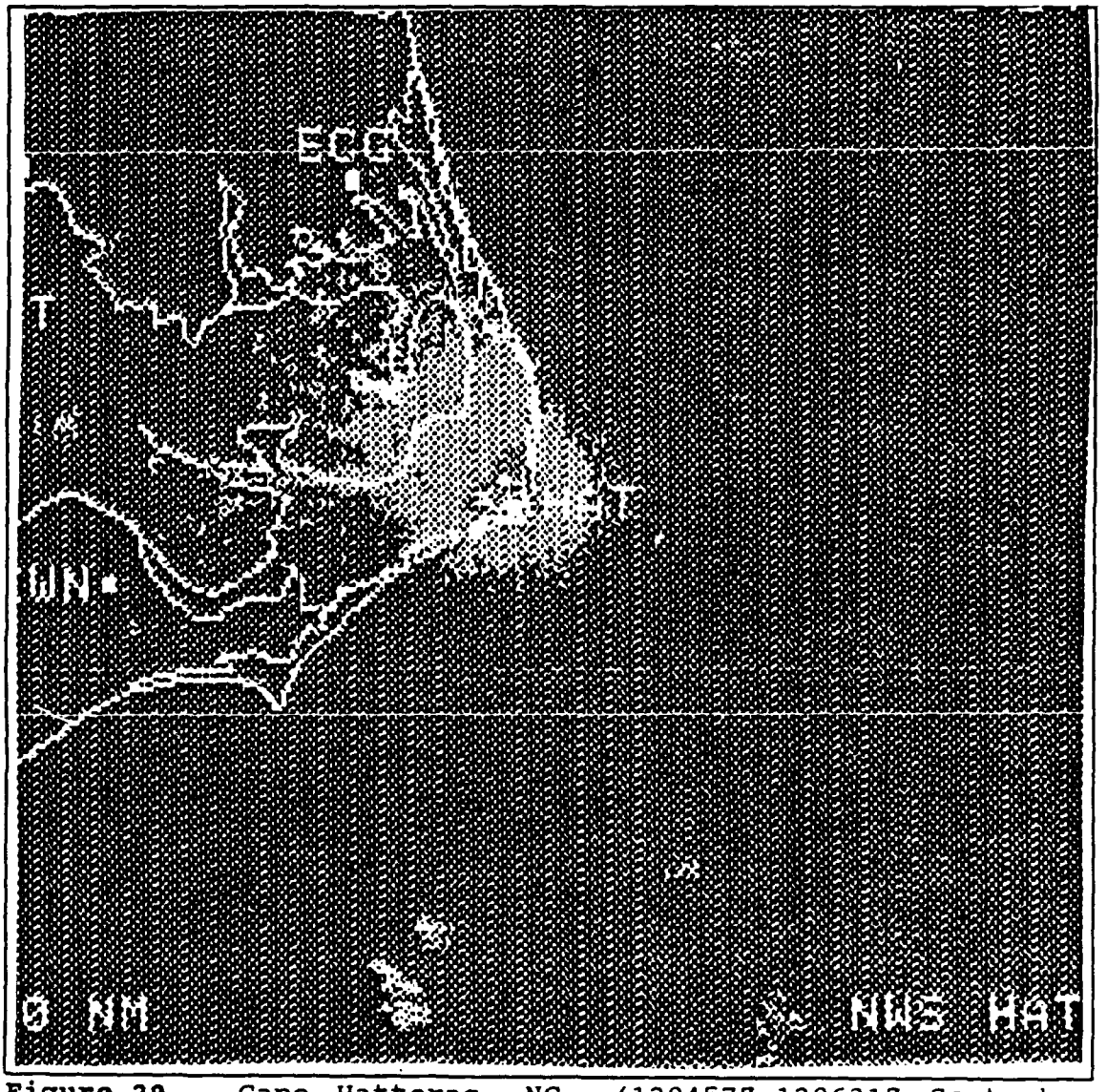

Figure 29. Cape Hatteras, NC (120457Z-120631Z September 1991).

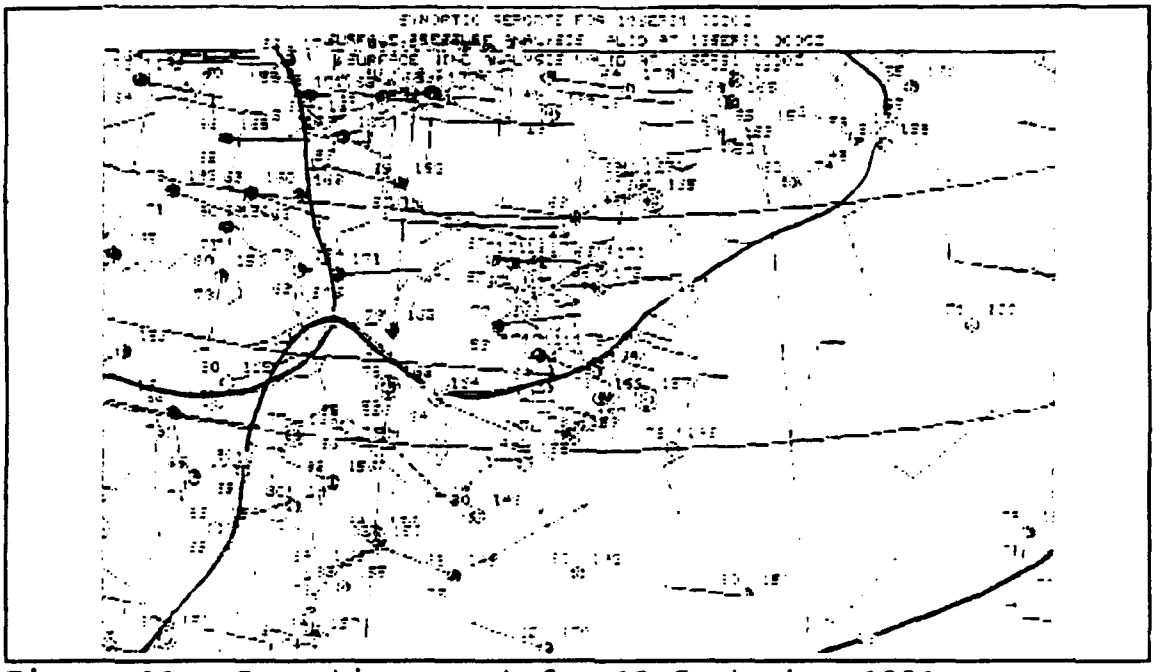

Figure 30. Synoptic report for 12 September 1991.

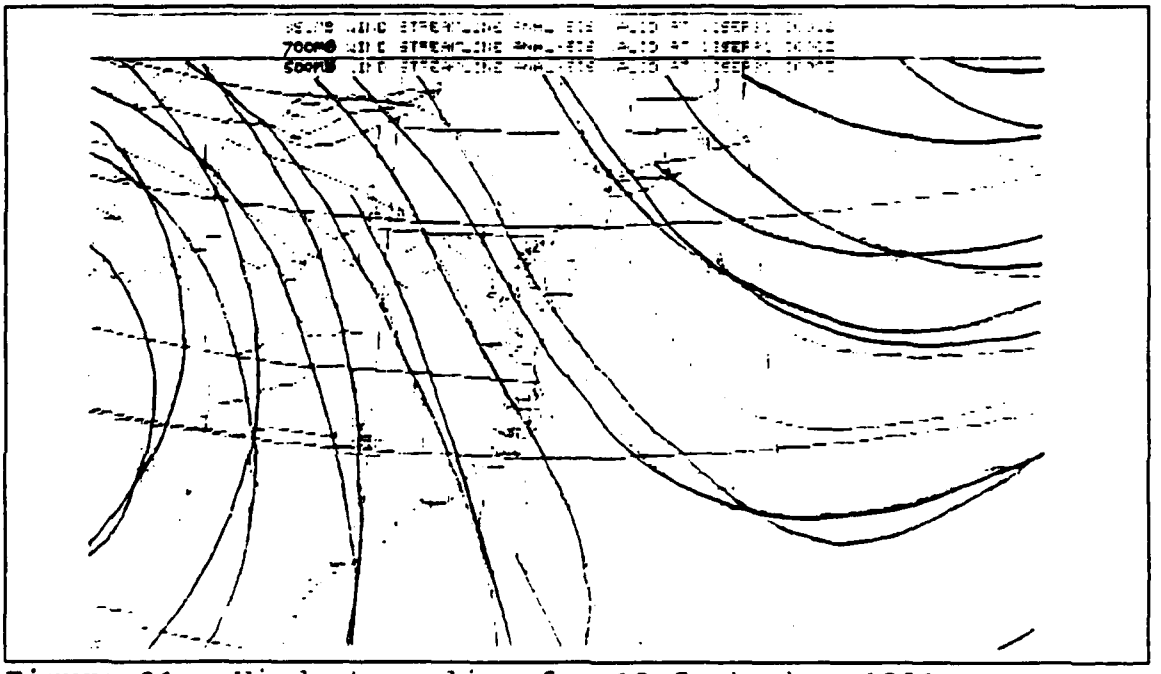

Figure 31. Wind streamline for 12 September 1991.

E. CASE #5 (14 September 1991)

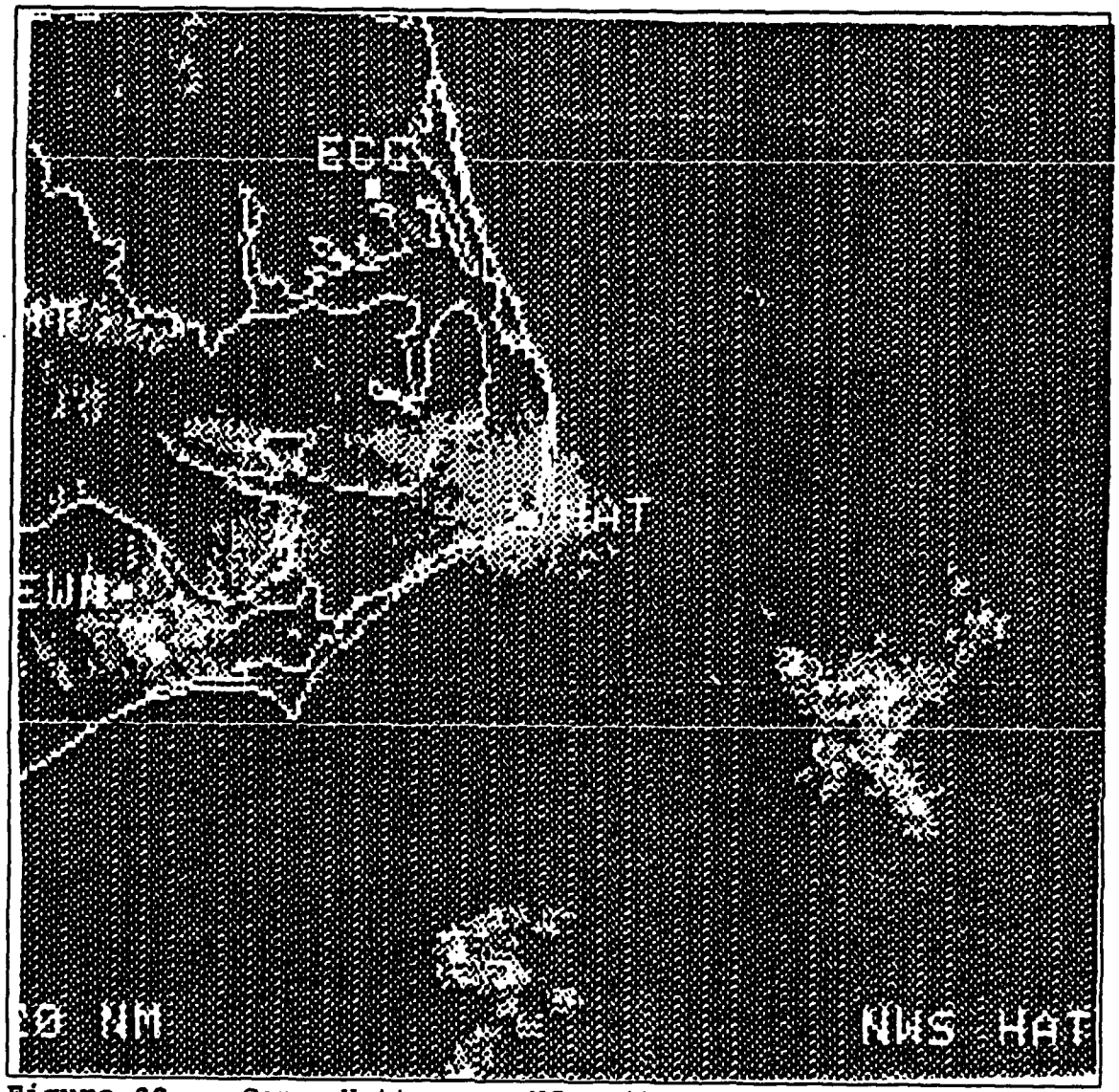

Figure 32. Cape Hatteras, NC (140536Z-140713Z September 1991).

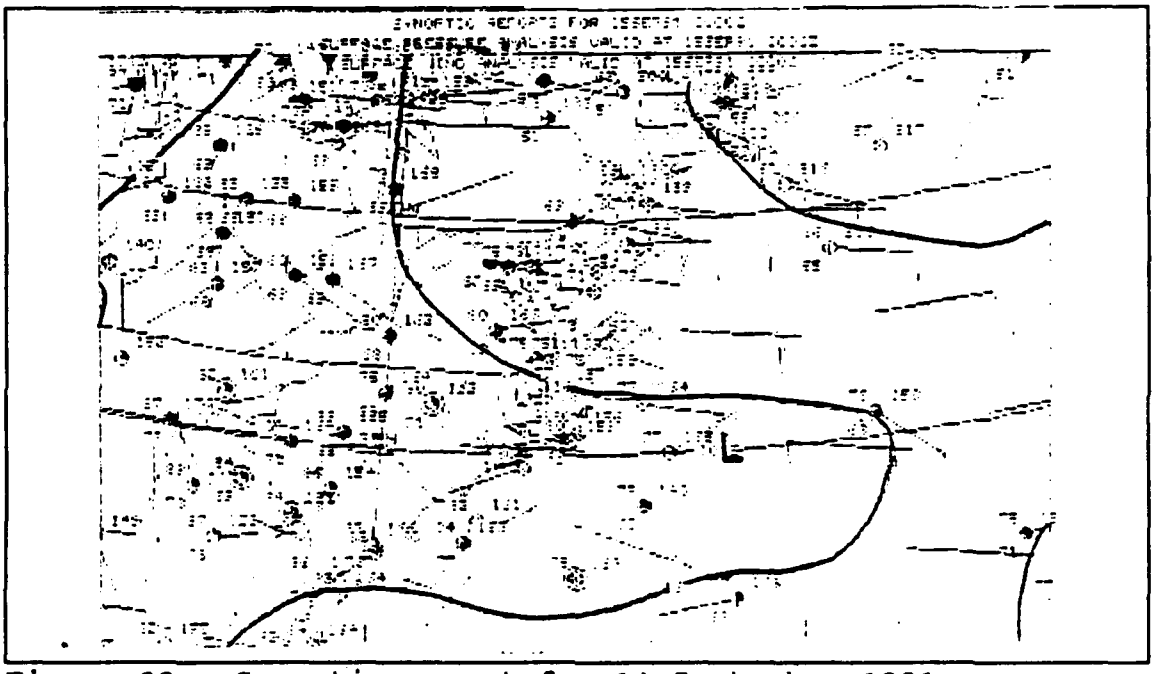

Figure 33. Synoptic report for 14 September 1991.

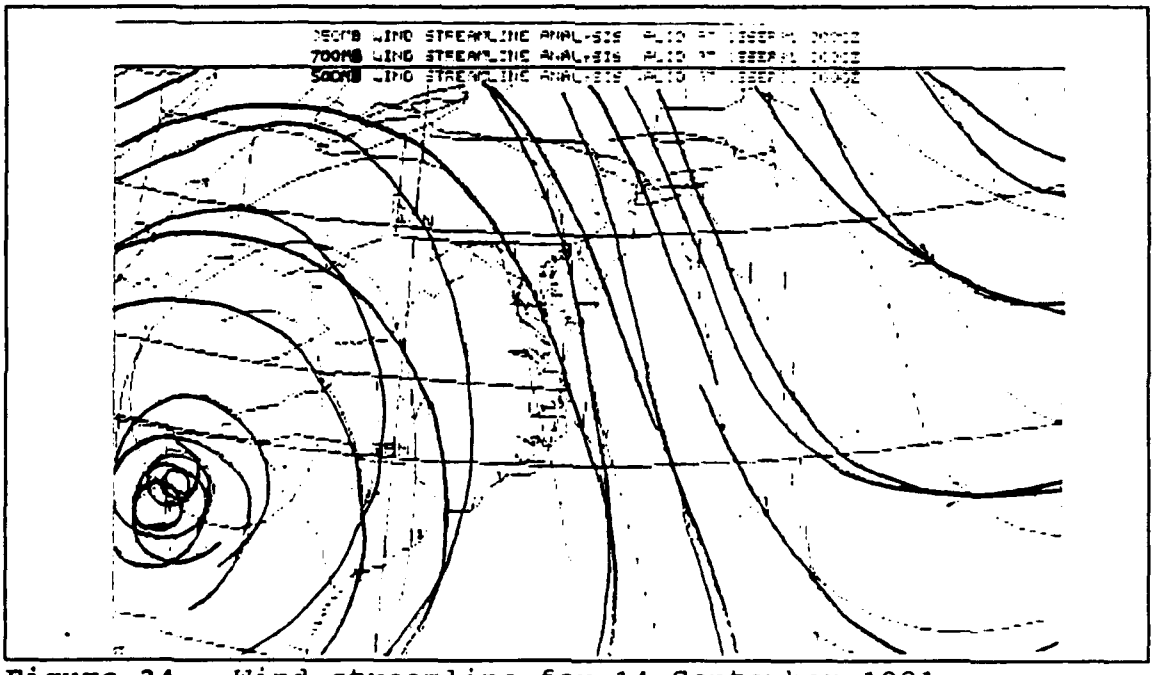

Figure 34. Wind streamline for 14 September 1991.

F. CASE #6 (02 October 1991)

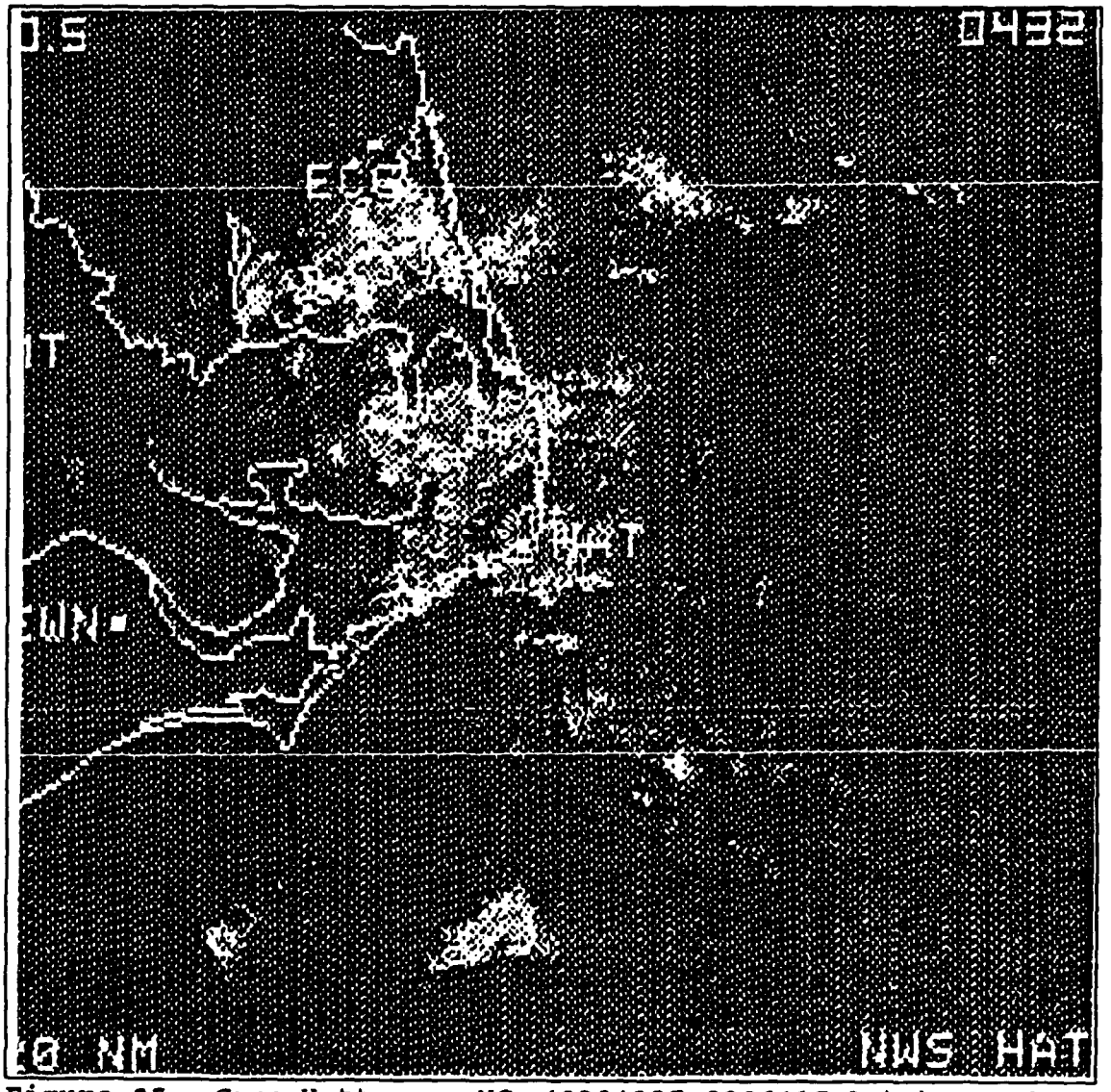

Figure 35. Cape Hatteras, NC (020432Z-020641Z October 1991).

APPENDIX C: Calculation for Kalman Filter Inputs

This thesis predicts the movement of the precipitation storm cells by updating the tracking algorithm using position-only data. The mathematical development of these equations is found in Reference 15. Historical data for the average velocity of precipitation storm cells was assumed to be approximately 8 nautical miles per hour. For simulation purposes the number of course changes per hour (β) was initially set at 4. Therefore the variables for the initial error covariance matrix to start the Kalman filter algorithm were calculated below:

$$\frac{\sigma^2}{\beta} = V^2$$

$$\sigma^2 = \beta\ V^2$$

$$\therefore \sigma = V\sqrt{\beta}$$

and

$$\sigma_{U_x}^2 = \sigma_{U_y}^2 = \frac{\sigma^2}{2\beta}$$

APPENDIX D. Kalman Filter Program

This Kalman filter program listing (written in 386-MATLAB) was used to predict the track of the centroid for the precipitation storm cells.

```
casesen off
%
%     This section sets up the initial prediction position, a
%     few other variables and sets up the storm data file to be used.
%

mum = [0 0 0 0]';
muw = [0 0 0 0]';
muv = [0 0 0 0]';

sigma = 1000000 * eye(4);

%
%     This is the data section of the program.  Only one set is
%     activated at a time.  All the other data sets are set to
%     comment statements.
%

% 10 Aug Storm #1

% measurements = [860 584 0 11
%                 867 576 11 0
%                 841 571 9 0
%                 887 556 9 0
%                 888 550 9 0
%                 906 520 8 0
%                 876 526 9 0
%                 896 517 8 0
%                 914 472 9 0
%                 913 463 9 0
%                 924 442 8 0];

% 10 Aug Storm #3

% measurements = [1252 786 0 12
%                 1265 768 11
%                 1253 778 9
%                 1255 727 9
%                 1262 722 9
%                 1255 686 8
%                 1273 684 9
%                 1298 668 8
%                 1261 593 11
%                 1289 604 9
%                 1290 574 8
%                 1284 561 8];

% 10 Aug Storm #4

% measurements = [1559 1170 0 10
%                 1558 1135 9 0
%                 1555 1103 9 0
%                 1572 1078 0 0
%                 1564 1086 9 0
%                 1562 1066 8 0
%                 1553 1021 11 0
%                 1556 1003 9 0
%                 1553 959 8 0
%                 1543 948 8 0];
```

```
% 18 Aug storm

% measurements = [529 1113 0 13
%                  492 1103 9 0
%                  464 1079 8 0
%                  413 1110 9 0
%                  396 1098 9 0
%                  360 1093 10 0
%                  331 1096 9 0
%                  289 1069 8 0
%                  294 1055 9 0
%                  267 1002 8 0
%                  246 1023 8 0
%                  221 994 9 0
%                  194 996 8 0];

% 10 Sep storm

      urements = [1344 1159 0 13
%                 1352 1144 10 0
%                 1357 1129 10 0
%                 1364 1117 10 0
%                      1116 10 0
%                           10 0
%                 13
%                 1340 10
%                 1346 1075
%                 1318 1068 10
%                 1333 1039 11 0
%                 1339 1032 11 0
%                 1322 1021 11 0];

% 31 Aug Storm

% measurements = [548 707 0 13
%                 568 713 10 0
%                 565 691 10 0
%                 575 657 10 0
%                 580 659 10 0
%                 569 643 10 0
%                 563 620 10 0
%                 598 607 12 0
%                 612 600 10 0
%                 636 596 10 0
%                 648 571 10 0
%                 711 558 10 0
%                 739 553 10 0];


% measurements
%                 1869 1603 9 0
%                 1883 1608 9 0
%                 1886 1618 8 0
%                 1904 1616 9 0
%                 1913 1600 8 0
%                 1920 1611 8 0
%                 1933 1605 9 0
%                 1942 1589 8 0
%                 1947 1579 9 0
```

```
%                  1944 1592 3 0
%                  1952 1591 9 0];

% 14 Sep Storm

% measurements = [1370 862 0 11
%                  1385 871 10 0
%                  1395 871 10 0
%                  1405 875 10 0
%                  1430 882 9 0
%                  1444 891 12 0
%                  1449 883 9 0
%                  1464 887 9 0
%                  1486 889 10 0
%                  1487 886 9 0
%                  1502 881 9 0];

% 2 Oct Storm

measurements = [390 1315 0 10
                422 1334 15 0
                442 1353 14 0
                474 1372 15 0
                501 1405 14 0
                524 1434 15 0
                537 1460 14 0
                565 1474 13 0
                612 1503 14 0
                647 1522 14 0];


%
%     This section initializes delta time from the data
%     set and the historical velocity of storm cells (V),
%     and values to be used to initially set the phi, Q,
%     and R matrix.
%

j = 2;

dt = measurements (j,3)/60;

V = 10;
alfa = 1/dt;
bravo = alfa;
tau = V * (sqrt(bravo));

a  = 5;
b = 5;
theta = 0;

phi = [1 0 dt 0
       0 1 0 dt
       0 0 1 0
       0 0 0 1];

q11 = (tau^2/(2*(bravo^2)))*(2*dt-((1/bravo)*(3-(4*exp(-bravo*dt))+exp(-2*br
q12 = (tau^2/(2*(bravo^2)))*(1-(2*exp(-bravo*dt))+exp(-2*bravo*dt));
q21 = q12;
q22 = (tau^2/(2*bravo)*(1-exp(-2*bravo*dt)));
```

```
Q = [q11 0 q12 0
     0 q11 0 q12
     q12 0 q22 0
     0 q21 0 q22];


r11 = 1/4*((a^2*(cos(theta))^2)+(b^2*(sin(theta))^2));
r12 = 1/4*((b^2-a^2)*sin(theta)*cos(theta));
r21 = r12;
r22 = 1/4*((a^2*(sin(theta)^2))+(b^2*(cos(theta)^2)));

R = [r11 r12 0 0
     r21 r22 0 0
     0 0 tau^2/(2*alfa) 0
     0 0 0 tau^2/(2*alfa)];

H = [1 0 0 0
     0 1 0 0
     0 0 0 0
     0 0 0 0];


%
%     This section allows the user to set the number of
%     storm cells radar data sets to use to initialize
%     the Kalman filter.
%

num = input('How many sets of data do you want to use to initialize the Kalman f


%
%     This section reads the storm cells data files where
%     the variables are (X-posit; Y-posit; Time)
%

x = [0 0 0 0]';
sigmam = sigma;

for i = 1:num;

     j = j + 1;

%
%     Compute the Kalman Gain (K)
%


     k = sigmam * h' * (h * sigmam * h' + r)^(-1);


%
%     Reads a radar position data set of the storm cell
%


     z1 = measurements (i,1);
     z2 = measurements (i,2);
```

```
      z = [z1 z2 0 0]';

%
%     updates the mean and std deviation and predicts the next
%     movement of the cell centroid.
%

      mup = mum + k * (z - muv -(h * mum));

      sigmap = sigmam * (eye(4) - (k * h));

      mum = phi * mup + muw;

      sigmam = phi * sigmap * phi' + q;

      phi(1,3) = measurements(j,3)/60;
      phi(2,4) = phi(1,3);

%
%     stores the radar data position and the kalman predition
%     position to use during the plotting of the storm cell.
%

pt1(i)=z(1,1);
pt2(i)=z(2,1);
pt3(i)=mum(1,1);
pt4(i)=mum(2,1);

end;

%
%     This section projects the storm cell's position based
%     on the calculated mean and std deviation from the past
%     cell positions used to initialize the Kalman filter.
%

l = 1;
k = num + 1;
     while k < measurements(1,4);
          realx(l) = measurements(k,1);
          realy(l) = measurements(k,2);
          finalx(l) = mum(1,1) + (mum(3,1) * (measurements(j,3)/60));
          finaly(l) = mum(2,1) + (mum(4,1) * (measurements(j,3)/60));
          mum(1,1) = finalx(l);
          mum(2,1) = finaly(l);
          j = j + 1;
          k = k + 1;
          l = l + 1;
     end;

%
%     predicts the final position of the storm cell centroid.
%
```

```
realx(1) = measurements(k,1);
realy(1) = measurements(k,2);
finalx(1) = mum(1,1) + (mum(3,1) * (measurements(j-1,3)/60) :
finaly(1) = mum(2,1) + (mum(4,1) * (measurements(j-1,3)/60) :


%
%     This section will generate the plotting function to display
%     the radar position of the storm cell and the Kalman filter's
%     predicted position.
%


plot(pt1,pt2,'+w',pt1,pt2,'-w',pt3,pt4,'or',pt3,pt4,'-r',realx,realy,'-w',realx,

title('storm cell movement (18Aug) x = actual | o = Kalman | * = projected');

xlabel('x-coordinates');

ylabel('y-coordinates');

pause;

j = 2;
dt = data(j,3)
mup = zeros(2,10);
mum =
end
```

APPENDIX E: STORM CELL LOCATION DATA (RADAR DETECTED/KALMAN PREDICTED)

The following tables are a summary of the results of the Kalman filter motion algorithm and a statistical weighted analysis of the storm cells growth and decay.

18 AUGUST 1991 (Initialized with Pts 1,2)							
TIME	RDR X	RDR Y	KALMAN X	KALMAN Y	Δ X	Δ Y	CENTROID ERROR
0446	529	1113	528.99	1113.0	-0.01	0.00	0.01
0455	492	1103	459.14	1094.1	-32.85	-8.90	34.03
0503	464	1079	422.16	1084.1	-41.83	+5.10	42.14
0512	413	1110	385.18	1074.1	-27.81	-35.90	45.37
0521	396	1098	344.10	1063.1	-51.89	-34.90	62.56
0531	360	1093	307.12	1053.1	-52.87	-39.90	66.25
0540	331	1096	274.26	1044.2	-56.73	-51.80	76.83
0548	289	1069	237.28	1034.2	-51.71	-34.80	62.33
0557	294	1055	204.41	1025.3	-89.58	-29.70	94.37
0605	267	1002	171.54	1016.4	-95.45	+14.40	96.53
0613	246	1023	134.57	1006.5	-111.4	-16.50	112.6
0622	221	994	101.70	997.6	-119.2	+3.60	119.3
0630	194	996	68.83	988.7	-125.1	-7.30	125.3

one *Image-Pro Plus* dimensionless unit equals approximately 240m

18 AUGUST 1991 (Initialized with Pts 1,2,3)							
TIME	RADAR X	RADAR Y	KALMAN X	KALMAN Y	Δ X	Δ Y	CENTROID ERROR
0446	529	1113	528.99	1113.0	-0.01	0.0	0.01
0455	492	1103	459.14	1094.1	-32.85	-8.9	34.03
0503	464	1079	429.59	1061.0	-34.40	-18.0	38.82
0512	413	1110	395.19	1043.0	-17.80	-67.0	69.31
0521	396	1098	356.96	1023.0	-39.03	-75.0	84.53
0531	360	1093	322.55	1005.0	-37.44	-87.0	94.71
0540	331	1096	291.97	989.0	-39.02	-107.0	113.8
0548	289	1069	257.57	971.0	-31.42	-98.0	102.91
0557	294	1055	226.99	955.0	-67.00	-100.0	120.37
0605	267	1002	196.40	939.0	-70.59	-63.0	94.610
0613	246	1023	162.00	921.0	-83.99	-102.0	132.13
0622	221	994	131.42	905.0	-89.57	-89.0	126.27
0630	194	996	100.84	889.1	-93.15	-106.9	141.79

one *Image-Pro Plus* dimensionless unit equals approximately 240m

31 AUGUST 1991 (Initialized with Pts 1,2,3)							
TIME	RADAR X	RADAR Y	KALMAN X	KALMAN Y	Δ X	Δ Y	CENTROID ERROR
0646	548	707	547.99	706.99	0.01	0.01	0.01
0656	568	713	587.99	719.00	19.99	6.00	20.87
0706	565	691	573.49	683.00	8.49	7.99	11.67
0716	575	657	581.99	675.00	6.99	18.00	19.31
0726	580	659	590.49	667.00	10.49	8.00	13.20
0736	569	643	598.99	659.00	29.99	16.00	34.00
0746	563	620	609.19	649.40	46.19	29.40	54.76
0758	598	607	617.69	641.40	19.69	34.40	39.64
0808	612	600	626.19	633.40	14.19	33.40	36.30
0818	636	596	634.69	625.41	1.30	29.41	29.43
0828	648	571	643.19	617.41	4.80	46.41	46.66
0838	711	558	651.69	609.41	59.30	51.41	78.48
0848	739	553	660.19	601.41	78.80	48.41	92.49

one *Image-Pro Plus* dimensionless unit equals approximately 240m

31 AUGUST 1991 (Initialized with Pts 7,8,9)							
TIME	RADAR	RADAR Y	KALMAN X	KALMAN Y	Δ X	Δ Y	CENTROID ERROR
0746	563	620	562.99	619.99	0.01	0.01	0.01
0758	598	607	627.15	596.17	1.82	10.82	31.09
0808	612	600	634.27	590.91	22.27	9.08	24.05
0818	636	596	656.54	581.82	20.54	14.17	24.96
0828	648	571	678.81	572.73	30.81	1.73	30.86
0838	711	558	701.08	563.64	9.91	5.64	11.40
0848	739	553	723.35	554.55	15.64	1.55	15.71

one *Image-Pro Plus* dimensionless unit equals approximately 240m

10 SEPTEMBER 1991 (Initialized with Pts 5,6,7,8)							
TIME	RADAR X	RADAR Y	KALMAN X	KALMAN Y	Δ X	Δ Y	CENTROID ERROR
0417	1367	1116	1367	1116	0	0	0
0427	1352	1117	1338.5	1117.9	-13.5	+.9	13.51
0436	1355	1110	1350	1107.5	-5	-2.5	5.64
0444	1340	1087	1329	1075.2	-11	-11.8	16.13
0455	1346	1075	1319	1064.4	-27	-10.6	28.97
0505	1318	1068	1308	1052.6	-10	-15.4	18.32
0516	1333	1039	1297	1040.8	-64	+1.2	36.02
0527	1339	1032	1286	1029.0	-53	-3	53.06
0538	1322	1021	1275	1017.2	-47	-3.8	47.12

one *Image-Pro Plus* dimensionless unit equals approximately 240m

12 SEPTEMBER 1991 (Initialized with Pts 1,2,3)							
TIME	RADAR X	RADAR Y	KALMAN X	KALMAN Y	Δ X	Δ Y	CENTROID ERROR
1860	1860	1608	1860	1608	0	0	0
1869	1869	1603	1878	1598	9	5	10.29
1883	1883	1608	1893.2	1608	10.2	0	10.2
1886	1886	1618	1904.7	1608	18.7	10	21.20
1904	1904	1616	1915	1608	11	8	13.60
1913	1913	1600	1925.2	1608	12.2	8	14.58
1920	1920	1611	1936.7	1608	16.7	3	16.96
1933	1933	1605	1946.9	1608	13.9	3	14.22
1942	1942	1589	1958.4	1608	16.4	19	25.09
1947	1947	1579	1968.6	1608	21.6	29	36.16
1944	1944	1592	1980.2	1608	36.2	16	39.57
1952	1952	1591	1991.7	1608.1	39.7	17	43.18

one *Image-Pro Plus* dimensionless unit equals approximately 240m

14 SEPTEMBER 1991 (Initialized with Pts 1,2,3)							
TIME	RADAR X	RADAR Y	KALMAN X	KALMAN Y	Δ X	Δ Y	CENTROID ERROR
0536	1370	862	1370	861.99	0	-0.01	0.01
0546	1384	871	1400	879.99	+16	+8.99	18.35
0556	1395	871	1407.5	875.50	+12.5	+4.50	13.28
0606	1405	875	1418.8	879.55	+13.8	+4.55	14.53
0615	1430	882	1433.8	884.95	+3.8	+2.95	4.81
0627	1444	891	1445.0	889.00	+1	-1.99	2.23
0636	1449	883	1456.3	893.05	+7.3	+10.05	12.42
0645	1464	887	1468.8	897.55	+4.8	+10.55	11.59
0655	1486	889	1480	901.61	-6	+12.61	13.96
0704	1487	886	1491.3	905.66	+4.3	+19.66	20.12
0713	1502	881	1502.5	909.71	+0.5	+28.71	28.71

one *Image-Pro Plus* dimensionless unit equals approximately 240m

02 OCTOBER 1991 (Initialized with Pts 1,2)							
TIME	RADAR X	RADAR Y	KALMAN X	KALMAN Y	Δ X	Δ Y	CENTROID ERROR
0432	390	1315	389.99	1315.0	-0.01	0.0	0.01
0447	422	1334	451.85	1351.7	+29.85	+17.7	34.71
0501	442	1353	483.85	1370.7	+41.85	+17.7	45.44
0516	474	1372	513.71	1388.5	+39.71	+16.5	43.00
0531	501	1405	545.71	1407.5	+44.71	+2.5	44.78
0546	524	1434	575.57	1425.2	+51.57	-8.8	52.32
0600	537	1460	603.30	1441.7	+66.30	-18.3	68.78
0613	565	1474	633.17	1459.4	+68.17	-14.6	69.71
0627	612	1503	663.03	1477.2	+51.03	-25.7	57.14
0641	647	1522	692.89	1494.9	+45.89	-27.1	53.30

one *Image-Pro Plus* dimensionless unit equals approximately 240m

02 OCTOBER 1991 (Initialized with Pts 1,2,3)							
TIME	RADAR X	RADAR Y	KALMAN X	KALMAN Y	Δ X	Δ Y	CENTROID ERROR
390	390	1315	389.99	1315.0	-0.01	0.0	0.01
422	422	1334	451.85	1351.7	+29.85	+17.7	34.71
442	442	1353	468.89	1372.7	+26.89	+19.7	33.33
474	474	1372	493.99	1391.0	+19.99	+19.0	27.58
501	501	1405	520.89	1410.7	+19.89	+5.7	20.69
524	524	1434	545.99	1429.0	+21.99	-5.0	22.55
537	537	1460	569.30	1446.1	+32.30	-13.9	35.17
565	565	1474	594.41	1464.4	+29.41	-5.6	30.93
612	612	1503	619.51	1482.7	+7.51	-20.3	21.64
647	647	1522	644.61	1501.1	-2.38	-20.9	21.03

one *Image-Pro Plus* dimensionless unit equals approximately 240m

02 OCTOBER 1991 (Initialized with Pts 1,2,3,4)							
TIME	RADAR X	RADAR Y	KALMAN X	KALMAN Y	Δ X	Δ Y	CENTROID ERROR
0432	390	1315	389.99	1315.0	-0.01	0.0	0.01
0447	422	1334	451.85	1351.7	+29.85	+17.7	34.71
0501	442	1353	468.89	1372.7	+26.89	+19.7	33.33
0516	474	1372	500.72	1390.1	+26.72	+18.1	32.27
0531	501	1405	529.36	1409.6	+28.36	+4.6	28.73
0546	524	1434	556.09	1427.7	+32.09	-6.3	32.70
0600	537	1460	580.90	1444.6	+43.90	-15.4	46.53
0613	565	1474	607.63	1462.7	+42.63	-11.3	44.10
0627	612	1503	634.36	1480.8	+22.36	-22.2	31.51
0641	647	1522	661.08	1499.9	+14.08	-22.1	26.20

one *Image-Pro Plus* dimensionless unit equals approximately 240m

APPENDIX F: STORM CELL SIZE DATA (MAJOR/MINOR AXIS: RADAR/STAT)

This appendix contains the data used with the simple statistical algorithm to predict the size of the major and minor axis. All table entries (except time) are normalized to *Image-Pro Plus* non-dimensional units. Each unit is approximately 240 meters.

18 AUGUST 1991					
TIME	RADAR MAJ	RADAR MIN	STAT MAJ	STAT MIN	CENTROID ERROR
0446	139.89	61.61	-	-	0.01
0455	131.92	76.21	-	-	34.03
0503	177.18	104.85	-	-	42.14
0512	160.16	79.27	-	-	45.37
0521	183.53	70.01	161.63	80.49	62.56
0531	179.23	82.77	163.26	81.84	66.25
0540	168.94	90.91	164.73	83.06	76.83
0548	146.37	97.81	166.04	84.14	62.33
0557	163.00	129.07	167.51	85.36	94.37
0605	102.81	75.26	168.82	86.44	96.53
0613	186.65	100.95	170.13	87.52	112.60
0622	189.10	65.70	171.60	88.74	119.30
0630	210.07	78.63	172.91	89.82	125.30

one *Image-Pro Plus* dimensionless unit equals approximately 240m

31 AUGUST 1991					
TIME	RADAR MAJ	RADAR MIN	STAT MAJ	STAT MIN	CENT ERROR
0646	88.61	71.78	-	-	0.01
0656	131.88	73.62	-	-	20.87
0706	138.25	77.43	-	-	11.67
0716	151.23	70.52	-	-	19.31
0726	146.55	80.36	155.40	80.29	13.20
0736	154.12	120.97	159.57	80.22	34.00
0746	166.89	100.41	163.74	80.15	54.76
0758	212.03	83.81	168.74	80.06	39.64
0808	210.93	78.29	173.91	79.99	36.30
0818	231.01	68.74	178.08	79.92	29.43
0828	199.92	66.32	182.25	79.85	46.66
0838	127.47	83.30	187.42	79.78	78.48
0848	145.53	93.98	191.59	79.71	92.49

one *Image-Pro Plus* dimensionless unit equals approximately 240m

10 SEPTEMBER 1991					
TIME	RADAR MAJ	RADAR MIN	STAT MAJ	STAT MIN	CENTROID ERROR
0417	187.57	76.81	-	-	0.0
0427	215.68	69.73	-	-	13.51
0436	224.84	63.38	224.81	69.60	5.64
0444	247.56	76.82	247.53	69.48	16.13
0455	200.26	110.23	247.49	69.32	28.97
0505	259.95	96.29	247.46	69.17	18.32
0516	180.92	96.10	247.42	69.01	36.02
0527	170.52	89.98	247.38	68.85	53.06
0538	204.16	78.27	247.34	68.69	47.12

one *Image-Pro Plus* dimensionless unit equals approximately 240m

12 SEPTEMBER 1991					
TIME	RADAR MAJ	RADAR MIN	STAT MAJ	STAT MIN	CENTROID ERROR
0457	131.68	60.98	-	-	0.00
0506	127.84	58.55	-	-	10.29
0515	135.60	64.01	-	-	10.20
0523	145.78	60.51	-	-	21.20
0532	174.87	66.94	146.75	60.34	13.60
0540	159.05	57.46	147.61	60.19	14.58
0548	164.62	64.73	148.47	60.04	16.96
0557	167.85	64.47	149.44	59.86	14.22
0605	159.63	76.92	150.30	59.71	25.09
0614	162.45	74.22	151.27	59.54	36.16
0622	162.47	77.38	152.13	59.39	39.57
0631	133.85	77.57	153.10	59.22	43.18

one *Image-Pro Plus* dimensionless unit equals approximately 240m

14 SEPTEMBER 1991					
TIME	RADAR MAJ	RADAR MIN	STAT MAJ	STAT MIN	CENT ERROR
0536	292.57	276.22	-	-	0.01
0546	298.05	211.96	-	-	18.35
0556	300.31	195.77	-	-	13.28
0606	309.44	187.52	-	-	14.53
0615	344.70	171.87	-	-	4.81
0627	342.25	175.32	345.46	167.11	2.23
0636	358.07	156.05	347.24	163.54	12.42
0645	372.77	162.37	349.02	159.97	11.59
0655	376.02	181.65	351.00	156.01	13.96
0704	374.42	173.98	352.78	152.44	20.12
0713	371.24	163.92	354.56	148.87	28.71

one *Image-Pro Plus* dimensionless unit equals approximately 240m

02 OCTOBER 1991					
TIME	RADAR MAJ	RADAR MIN	STAT MAJ	STAT MIN	CENTROID ERROR
0432	191.58	101.42	-	-	0.01
0447	218.45	88.48	-	-	34.71
0501	204.10	80.53	-	-	33.33
0516	221.64	84.15	-	-	27.58
0531	200.44	89.94	-	-	20.69
0546	212.77	82.69	200.77	89.50	22.55
0600	147.15	84.23	201.08	89.1	35.17
0613	135.01	86.93	201.37	88.72	30.93
0627	137.80	62.40	201.68	88.32	21.64
0641	144.88	99.14	201.99	87.92	21.03

one *Image-Pro Plus* dimensionless unit equals approximately 240m

APPENDIX G: STORM CELL ORIENT (θ) DATA (MAJOR AXIS: RADAR/STAT)

The following tables are a summary of the results of a statistical weighted analysis of the storm cells major axis orientation (θ) rotation.

18 AUGUST 1991		
TIME	RADAR THETA (θ)	STATISTICAL THETA (θ)
0446	134	-
0455	136	-
0503	163	-
0512	213	-
0521	206	217
0531	192	221
0540	189	225
0548	216	229
0557	188	234
0605	252	240
0613	350	244
0622	347	248
0630	345	252

31 AUGUST 1991		
TIME	RADAR THETA (θ)	STATISTICAL THETA (θ)
0646	006	-
0656	162	-
0706	158	-
0716	157	-
0726	151	155
0736	122	153
0746	107	151
0758	105	149
0808	100	147
0818	105	145
0828	094	143
0838	111	141
0848	151	139

10 SEPTEMBER 1991		
TIME	RADAR THETA (θ)	STATISTICAL THETA (θ)
0337	085	-
0347	086	-
0357	093	-
0407	092	-
0417	089	-
0427	092	-
0436	090	092
0444	090	092
0455	092	093
0505	088	093
0516	100	094
0527	106	094
0538	108	095

12 SEPTEMBER 1991		
TIME	RADAR THETA (θ)	STATISTICAL THETA (θ)
0457	058	-
0506	062	-
0515	064	-
0523	066	-
0532	067	-
0540	073	067
0548	062	068
0557	067	068
0605	043	069
0614	040	069
0622	040	070
0631	045	070

14 SEPTEMBER 1991		
TIME	RADAR THETA (θ)	STATISTICAL THETA (θ)
0536	094	-
0546	055	-
0556	049	-
0606	046	-
0615	045	-
0627	042	043
0636	040	041
0645	038	039
0655	036	037
0704	033	035
0713	032	033

02 OCTOBER 1991		
TIME	RADAR THETA (θ)	STATISTICAL THETA (θ)
0432	159	-
0447	152	-
0501	143	-
0516	142	-
0531	136	141
0546	134	140
0600	147	139
0613	141	138
0627	038	137
0641	046	136

LIST OF REFERENCES

1. Pastore, M.J., *IOTA Demonstration at Sea* (preliminary point paper), April 1991.

2. USS Miller Naval Message, Subject: IOTA Demo at Sea I,221540Z Jul 90.

3. Hiser, H.W., and Freseman, W.L., *Radar Meteorology*, 2d ed., pp. 108-130, 1959.

4. Gossard, E.E., and Strauch R.G., *Radar Observation of Clear Air and Clouds*, pp. 107-115, 1983.

5. Crane, R.K., *Automatic Cell Detection and Tracking*, 1979.

6. Forsyth, D.E., *Real Time Forecasting of Echo-Centroid Motion*, Master's Thesis, University of Oklahoma, Norman, OK, 1979.

7. Conlee, D.T.,*Satellite Image Display and Processing with Microcomputers: A proof-of-concept for the navy Oceanographic data distribution system (NODDS)*, Master's Thesis, Naval Postgraduate School, Monterey, CA, pp. 3-8, June 1991.

8. Media Cybernetics Inc., *Image-Pro Plus User's Manual*, Version 1.0, 1991.

9. Washburn, A., "*A Short Introduction to Kalman Filters*",lecture notes taught at the Naval Postgraduate School Monterey, California, 19 June 1990.

10. Naval Surface Warfare Center Technical Report NSWC-TR-88-123, *Mathematical Analysis of the Maneuvering Target Statistical Tracker (MTST) System*, by D.H. McCabe, August 1988.

11. Sorenson, H.W., ed., *Kalman Filtering: Theory and Applications*, IEEE Press, 1985.

12. Gelb, A., *Applied Optimal Estimation*, MIT Press, Cambridge MA, 1974.

13. Byers, H.R., "*General Meteorology*",3rd ed, Mcgraw-Hill Book Co, 1959.

14. Kavouras Inc.,*RADAC User's Manual*, rev. E, 1984.

15. Vebber, P., *An Examination of Target Tracking in the Antisubmarine Warfare System Evaluation Tool (ASSET)*, Master's Thesis, Naval Postgraduate School, Monterey, CA, September 1991.

INITIAL DISTRIBUTION LIST

1.	Defense Technical Information Center Cameron Station Alexandria, Virginia 22304-6145	2
2.	Library, Code 52 Naval Postgraduate School Monterey, California 93943-5002	2
3.	Prof. C. H. Wash (Code MR/Wx) Department of Meteorology Naval Postgraduate School Monterey, California 93943-5005	1
4.	M. J. Pastore Naval Research Laboratory Monterey, California 93943-5006	1
5.	Dr A. K. Goroch Naval Research Laboratory Monterey, California 93943-5006	1
6.	LCDR W. J. Walsh 601 S. 6th St Princeton, Minnesota 55371	1
7.	LCDR C. A. Carpenter 2511 Meadow Lark Dr San Diego, California 92124	1
8.	S. Dasinger NUWC New London, Conneticutt 06320	1
9.	CAPT J. Seeley SWDG Little Creek, Virginia 23521-5160	1
10.	R. Winokur OP096 US Naval Observatory 34th & Massachuset Ave NW Washington, DC 20362-5160	1
11.	P. Tiedeman NAVSEA Code 06UR3 Washington, DC 20362-5160	1

12. P. Gilmer
Kavouras, INC.
6301 34th Ave South
Minneapolis, Minnesota 55450

1